Initiation of shear instability in three-dimensional elastodynamics

Pascal Favreau[1] and Michel Campillo

Laboratoire de Géophysique Interne, Observatoire de Grenoble, Université Joseph Fourier, Cedex, France

Ioan R. Ionescu

Laboratoire de Mathématiques Appliquées, Université de Savoie, Campus Scientifique, Cedex, France

[1] Earthquake nucleation may begin with a stable quasi-static localization of fault slip. This long-term process, which conditions the fault for the rupture, is followed by a dynamic and unstable phase that we call initiation and ends with the onset of rupture propagation. In this paper, we investigate the three-dimensional elastodynamics of this unstable initiation phase both analytically and numerically. The fault model consists of two symmetric semi-infinite elastic bodies in frictional contact across a flat interface with a slip-weakening law and loaded until its sliding threshold is reached. On the basis of our previous studies in two dimensions, we generalize the linear stability and the spectral analysis and then solve analytically the "dominant part" approximation for the homogeneous infinite fault. We then derive the slip pattern on the fault, the decay of the displacement amplitude in the media, and its growth in time. The model also gives a theoretical approximation for the time of initiation. To test the dominant part approximation, we compare it with the numerical solution in the case of a concentrated perturbation. Finally, we find that unlike the infinite fault, finite faults of a given geometry allow a domain of stability that depends on the fault size. When a finite fault becomes unstable and rupture initiates, the slip growth is determined by a single dominant eigenmode. The duration of the initiation phase varies strongly with the size and geometry of the fault, especially when it is close to the stability limit. *INDEX TERMS:* 1035 Geochemistry: Geochronology; 1094 Geochemistry: Instruments and techniques; 3660 Mineralogy and Petrology: Metamorphic petrology; 8110 Tectonophysics: Continental tectonics—general(0905); 9320 Information Related to Geographic Region: Asia; *KEYWORDS:* source, initiation, elastodynamics, friction law, instability, dominant part

1. Introduction

[2] Earthquakes are commonly associated with the propagation of fault rupture, an unstable process that radiates the observable seismic energy. This rupture is supposed to be primed by a nucleation process. Earthquake nucleation on faults is itself a complex process and must be conceptually divided into two successive phases. At first, the external tectonic loading drives a progressive quasi-static and stable slip localization on the fault. The duration of this phase depends on the strain rate and the complex frictional behavior on the fault. Slip occurs at a very low velocity, which allows for the renewing of individual contacts. This phase may last for many years [*Rice*, 1993; *Dieterich*, 1992; *Matsu'ura et al.*, 1992]. In the second phase the fault loses its stability and the slip grows at rates almost independent of the external load. We call this process initiation. To summa-rize, initiation is part of the crucial transition in nucleation from the quasi-static slow stage to the rapid crack propagation stage that generates the strong ground motions; it is the onset of rupture. This paper is devoted entirely to this particular phase of the rupture.

[3] Before addressing the details, we must avoid confusing the dynamic process, the radiative process, and the unstable process. For us, a dynamic process involves inertial forces (mass and acceleration). A radiative process emits a signal composed of propagative oscillatory waves (and nonradiative does not mean a lack of signal). An unstable process relies on a huge amplification of the field variables (displacement, stress, and others). These things are separate a priori, and one of them does not imply any of the others. For example, a precursory slip can be nonradiative and dynamic but still stable. Basically, the initiation is by definition an instability. In our model it also requires dynamics. As we will demonstrate, it is theoretically a nonradiative process which produces a tiny signal like any deformation process. In the laboratory, *Ohnaka and Shen* [1999] observed this phase when conducting locally monitored failure experiments between blocks of rock. *Iio* [1992]

---

[1]Now at the Institute for Crustal Studies, University of California at Santa Barbara, Santa Barbara, California, USA.

FAULT PLANE Γ_f :
$\sigma_{xz}(t,x,y,0)=f(\delta u_x(t,x,y))$
$\delta u_y(t,x,y)=0$
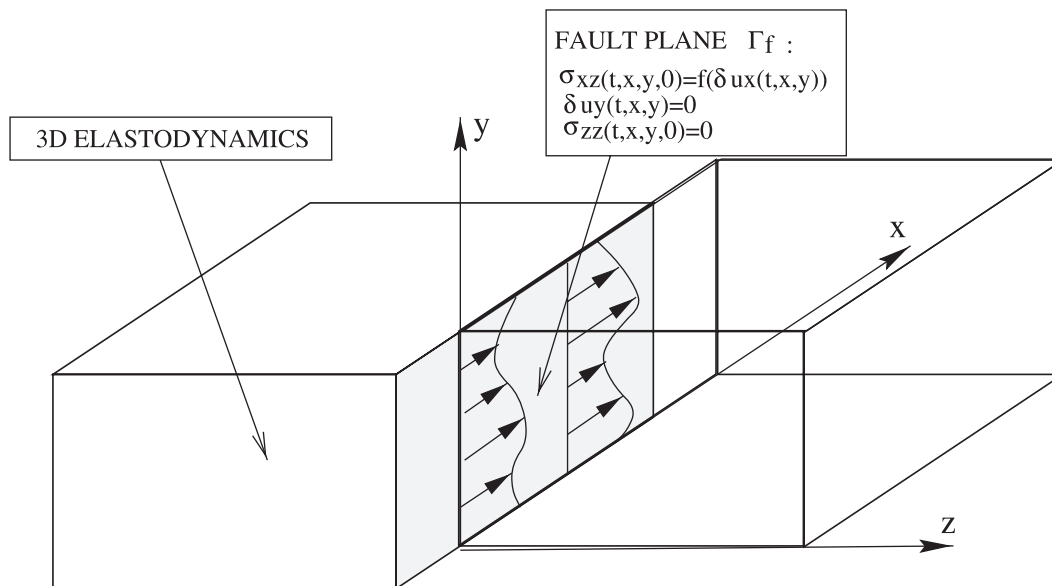$\sigma_{zz}(t,x,y,0)=0$

3D ELASTODYNAMICS

Figure 1. The 3-D problem and notation. The fault is a planar discontinuity inside an infinite elastic bulk. On the fault, normal stress is constant and the slip has a constant rake along x. When slipping, the shear stress acting on the fault along x is bounded by a slip-dependent friction law.

and *Ellsworth and Beroza* [1995] found evidence in seismograms of dynamic nucleation phases that may be related to an initiation process. The slow initial phase of seismograms has also been reobserved recently and positively identified as source effects by *Iio et al.* [1999].

[4] Several models of earthquake nucleation have been developed in two dimensions, but none exist within the context of three-dimensional (3-D) elastodynamics. To understand the complexity of the source nucleation process in the seismological context, it is necessary to construct a 3-D elastodynamic model of the initiation phase. In this work we propose to set up its mechanical base, the growth of a slip instability at constant rake on a fault plane in a 3-D elastic bulk. The fault strength is given by a slip-dependent constitutive law.

[5] The slip-dependent strength has been identified as a key process in both experimental and theoretical research on the rupture mechanism. In theoretical and numerical works this law was proposed previously by *Ida* [1972] and *Andrews* [1976a, 1976b] to model crack propagation in two dimensions. *Ohnaka et al.* [1987] succeeded in observing and measuring the slip-dependent process at the crack tips in two-dimensional laboratory experiments. *Olsen et al.* [1997] and *Madariaga et al.* [1998] used that relation in 3-D numerical models of the rupture process for large earthquakes. In their experiments they confirm that the critical slip-weakening distance contained in the slip-dependent friction is crucial. Indeed, it removes the singular behavior at the tip of the rupture, and it creates a breakdown zone at the rupture front where stress decreases progressively. In addition, it gives the size of the numerical discretization needed for conducting accurate numerical studies of rupture propagation. Furthermore, with slip-dependent friction and an initial stress heterogeneity (asperity model), *Peyrat et al.* [2001] construct a dynamical model of the 1992 Landers earthquake that fits the near-field

strong motion data in the frequency band 0−0.5 Hz. Recently, *Ohnaka* [1996] confirmed that the slip-weakening process is not only operating in the breakdown zone of the propagation process but also in the nucleation process. We must mention other laboratory-derived friction laws based on the rate-and-state framework. The rate-and-state friction laws are essential for the understanding of the long-term viscous fault creep [see *Rice and Ruina*, 1983; *Dieterich*, 1992]. Nevertheless, it is well recognized that the characteristic slip contained in the rate-and-state laws plays the same role as the critical slip-weakening distance in the slip-dependent friction laws. *Campillo and Ionescu* [1997] use the slip-weakening friction law to set up a theoretical initiation model for a two-dimensional (2-D) antiplane infinite fault. They find an analytical expression for the slip on an homogeneous fault, and they show that it is essentially dominated by a small part of the solution, "the dominant part" approximation, that contains only the unstable modes. An extension of that study in the 2-D in-plane case was performed by *Favreau et al.* [1999]. Furthermore, in the antiplane geometry, *Ionescu and Campillo* [1999] quantified the effect of the finiteness of a fault on the time of initiation; *Dascalu et al.* [2000] analytically justified this result as well.

[6] Here our goal consists of generalizing our previous findings in 2-D to the 3-D case. Section 2 presents the mechanical and mathematical problem statement. In section 3 we analytically and numerically study the initiation process on the infinite fault (a smooth fault). We generalize the concepts of spectral analysis and dominant part in three dimensions. We define the 3-D slipping patch, P_c. Appendices A, B, C, and D contain some technical aspects of that study. In section 4 we study the effect of fault finiteness in three dimensions. We numerically evaluate the stability limit and the eigenvalue of the first unstable mode of 3-D finite faults. In Appendix E we link
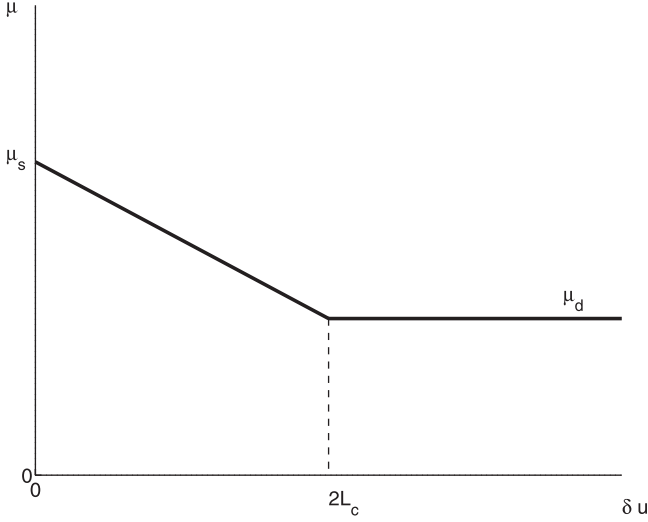
Figure 2. The slip-dependent friction law. Three para-meters, μ_s (static friction coefficient), μ_d (dynamic friction coefficient), and $2L_c$ (critical slip-weakening distance), define the idealized slip-dependent friction law.

the results with those found previously for 2-D finite faults.

2. The Problem Statement

[7] We consider the three-dimensional shearing of two homogeneous half-spaces bounded by the plane Γ_f at $z = 0$ (Figure 1). The half-spaces are in contact on a flat surface with slip-dependent friction and constant rake along x. The elastic medium has the density ρ and the two wave velocities v_p for P waves and v_s for S waves. The corresponding first Lamé coefficient is $\rho(v_p^2 - 2v_s^2)$ and the second one (the shear modulus) is ρv_s^2. By $\Phi(t, x, y, z)$ and $\Psi_i(t, x, y, z)$, $i = (x, y, z)$ we denote the Helmoltz potentials (corresponding to P and S waves). The displacement $u_i(x, y, z, t)$, $i = (x, y, z)$ and the stress fields acting on the fault $\sigma_{iz}(x, y, z, t)$, $i = (x, y, z)$ can be derived from the potentials as follows

$$u_x = \frac{\partial \Phi}{\partial x} + \frac{\partial \Psi_z}{\partial y} - \frac{\partial \Psi_y}{\partial z}, \; u_y = \frac{\partial \Phi}{\partial y} + \frac{\partial \Psi_x}{\partial z} - \frac{\partial \Psi_z}{\partial x},$$

$$u_z = \frac{\partial \Phi}{\partial z} + \frac{\partial \Psi_y}{\partial x} - \frac{\partial \Psi_x}{\partial y} \tag{1}$$

$$\frac{\sigma_{xz}}{\rho v_s^2} = 2\frac{\partial^2 \Phi}{\partial x \partial z} + \frac{\partial^2 \Psi_z}{\partial y \partial z} - \frac{\partial^2 \Psi_x}{\partial x \partial y} + \frac{\partial^2 \Psi_y}{\partial x^2} - \frac{\partial^2 \Psi_y}{\partial z^2} + \frac{\sigma_{xz}^\infty}{\rho v_s^2} \tag{2}$$

$$\frac{\sigma_{yz}}{\rho v_s^2} = 2\frac{\partial^2 \Phi}{\partial y \partial z} - \frac{\partial^2 \Psi_z}{\partial x \partial z} + \frac{\partial^2 \Psi_y}{\partial x \partial y} - \frac{\partial^2 \Psi_x}{\partial y^2} + \frac{\partial^2 \Psi_x}{\partial z^2} + \frac{\sigma_{yz}^\infty}{\rho v_s^2} \tag{3}$$

$$\frac{\sigma_{zz}}{\rho v_s^2} = (\eta^2 - 2)\left(\frac{\partial^2 \Phi}{\partial x^2} + \frac{\partial^2 \Phi}{\partial y^2} + \frac{\partial^2 \Phi}{\partial z^2}\right) + 2\left(\frac{\partial^2 \Phi}{\partial z^2} + \frac{\partial^2 \Psi_y}{\partial x \partial z} - \frac{\partial^2 \Psi_x}{\partial y \partial z}\right)$$
$$+ \frac{\sigma_{zz}^\infty}{\rho v_s^2}, \tag{4}$$

where σ_{iz}^∞, $i = (x, y, z)$ is the homogeneous static initial stress field acting on the whole domain. The ratio of P wave to S wave velocities is denoted by $\eta = v_p/v_s$. In a homogeneous infinite elastic bulk the equations of elastodynamics can be written as two separate wave equations,

$$\frac{\partial^2 \Phi}{\partial t^2} = v_p^2 \left(\frac{\partial^2 \Phi}{\partial x^2} + \frac{\partial^2 \Phi}{\partial y^2} + \frac{\partial^2 \Phi}{\partial z^2}\right),$$
$$\frac{\partial^2 \Psi_i}{\partial t^2} = v_s^2 \left(\frac{\partial^2 \Psi_i}{\partial x^2} + \frac{\partial^2 \Psi_i}{\partial y^2} + \frac{\partial^2 \Psi_i}{\partial z^2}\right), \; i = (x, y, z). \tag{5}$$

To obtain a unique potential Ψ_i, $i = (x, y, z)$, we add the classical Helmoltz condition

$$\frac{\partial \Psi_x}{\partial x} + \frac{\partial \Psi_y}{\partial y} + \frac{\partial \Psi_z}{\partial z} = 0. \tag{6}$$

We define the components of the fault slip by $\delta u_i(t, x, y) = u_i(t, x, y, 0^+) - u_i(t, x, y, 0^-)$, $i = (x, y, z)$ and the components of the fault slip velocity by $\delta v_i(t, x, y) = v_i(t, x, y, 0^+) - v_i(t, x, y, 0^-)$, $i = (x, y, z)$. The symmetries of the displacement are $u_i(t, x, y, -z) = -u_i(t, x, y, z)$, $i = (x, y)$ and $u_z(t, x, y, -z) = u_z(t, x, y, z)$. Therefore $\delta u_i(t, x, y) = 2u_i(t, x, y, 0^+)$, $i = (x, y)$ and $\delta u_z(t, x, y) = 0 \Rightarrow u_z(t, x, y, -z) = u_z(t, x, y, z) = 0$, which means that the fault does not open during the slip (i.e., no mode 1). The symmetries of the stress components acting on the fault are $\sigma_{iz}(t, x, y, -z) = \sigma_{iz}(t, x, y, z)$, $i = (x, y)$ and $\sigma_{zz}(t, x, y, -z) + \sigma_{zz}(t, x, y, z) = 2\sigma_{zz}^\infty$. The consequence of this last symmetry condition is a constant normal stress σ_{zz} on the fault plane during the slip (see condition (8)). This condition of symmetry may be violated for different geometrical (free surface, bent fault, etc.) or physical (contrast of density or elasticity across the fault) reasons. We do not consider these things in this paper. The condition of continuity of the stress vector on the fault plane Γ_f gives

$$\sigma_{iz}(t, x, y, 0^-) = \sigma_{iz}(t, x, y, 0^+) = \sigma_{iz}(t, x, y, 0), i = (x, y) \tag{7}$$

$$\sigma_{zz}(t, x, y, 0^+) = \sigma_{zz}(t, x, y, 0^-) = \sigma_{zz}(t, x, y, 0) = \sigma_{zz}^\infty. \tag{8}$$

The slip is in the direction x, and consequently we impose

$$\delta u_y(t, x, y) = 0 \Longrightarrow u_y(t, x, y, 0^+) = u_y(t, x, y, 0^-) = 0. \tag{9}$$

This means that the rake is constant. The traction drop has two components, σ_{xz} and σ_{yz}, and the resultant is not parallel to the slip. A vector friction could be used; however, many large earthquakes, particularly on pure strike-slip faults, seem to have a quasi-constant rake. Finally, if we assume that the initial stress is mainly oriented along x, i.e., $|\sigma_{xz}^\infty| \gg |\sigma_{yz}^\infty|$, then the angle of the total stress will not deviate from the direction x, the one of the slip. Assuming such rake, the frictional slip-dependent boundary condition on the fault plane Γ_f is scalar, and we write it as

$$\sigma_{xz}(t, x, y, 0) = -\sigma_{zz}^\infty \mu(x, y, \delta u_x(t, x, y)) \text{sign}(\delta v_x(t, x, y))$$
$$\text{if} \quad \delta v_x(t, x, y) \neq 0 \tag{10}$$

$$|\sigma_{xz}(t, x, y, 0)| \leq -\sigma_{zz}^\infty \mu(x, y, \delta u_x(t, x, y)) \quad \text{if} \quad \delta v_x(t, x, y) = 0, \tag{11}$$
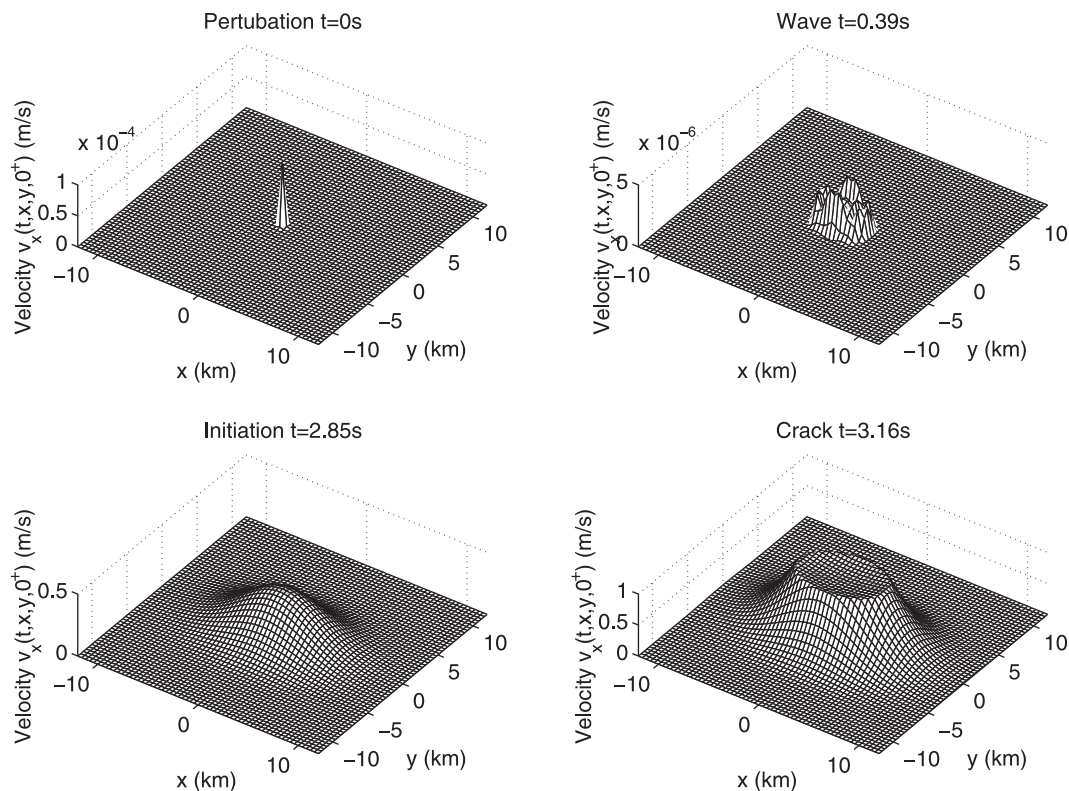
Figure 3. The slip velocity process on an infinite fault. After the propagation of the triggering perturbation (perturbation and wave generated by itself), the slip velocity grows by following a special stationary shape. This corresponds to the initiation. We study analytically the initiation by a spectral analysis. When the critical slip is reached, the crack regime begins. Numerical values are $\rho = 3000 \text{kgm}^{-3}$, $v_s = 3333 \text{ms}^{-1}$, $\eta = v_p/v_s = \sqrt{3}$, $\sigma_s - \sigma_d = 10 \text{MPa}$, and $L_c = 0.18$ m.

where $\mu(x, y, \delta u_x)$ is the slip-dependent friction coefficient. We assume that a backward slip rate is forbidden, i.e., $\delta v_x(t, x, y) \geq 0$. Since the initial slip is null, we have $\delta u_x(t, x, y) \geq 0$ as well. We consider in this paper only the case of a friction law with a piecewise linear dependence on the slip

$$\mu(\delta u_x) = \mu_s - \frac{\mu_s - \mu_d}{2L_c} \delta u_x \quad \text{if} \quad 0 \leq \delta u_x \leq 2L_c \quad (12)$$

$$\mu(\delta u_x) = \mu_d \quad \text{if} \quad \delta u_x > 2L_c. \quad (13)$$

This law (see Figure 2) is an idealization of the laws obtained in dynamic rupture laboratory experiments performed by *Ohnaka et al.* [1987]. Let us define the parameter α_c, which controls the initiation process and is the rate of strength weakening of the fault divided by the shear modulus of the bulk

$$\alpha_c = -\sigma_{zz}^\infty \frac{\mu_s - \mu_d}{\rho v_s^2 L_c} = \frac{\sigma_s - \sigma_d}{\rho v_s^2 L_c}, \quad (14)$$

where σ_s and σ_d denote the common static and dynamic frictions, respectively. The value of α_c has the dimension of the inverse of a length. In every case in this study the system is put in an unstable equilibrium position and the evolution is triggered by a small perturbation of the velocity field. This small perturbation is our initial

condition, and it verifies the symmetries defined above. We denote it by

$$u_i^0(x, y, z) = u_i(0, x, y, z), i = (x, y, z)$$
$$v_i^0(x, y, z) = v_i(0, x, y, z), i = (x, y, z). \quad (15)$$

The system is now completely defined, and the symmetry implies that we can work on the half-space ($z \geq 0$). Finally, in every calculation we take the set of numerical values $\rho = 3000 \text{ kgm}^{-3}$, $v_s = 3333 \text{ ms}^{-1}$, $\eta = v_p/v_s = \sqrt{3}$, and $\sigma_s - \sigma_d = 10$ MPa.

3. The Infinite Fault Model

[8] The homogeneous infinite fault, or completely smooth fault, is a limiting case in which the fault has neither a strength barrier nor a stress asperity. This situation is very critical. It is an idealized case that exhibits the natural scaling properties of the rupture nucleation induced by a uniform slip weakening (this idealized case seems unrealistic, but the infinite fault approximation can be encountered in a two-step initiation in a periodic array of breakable barriers or in an increasing slip-weakening process, as shown by *Campillo et al.* [2001]). In this way the fault is at the rupture level everywhere; that is, the initial static stress is assumed to correspond to the static friction level everywhere on the fault plane. This imposes that σ_{xz}^∞
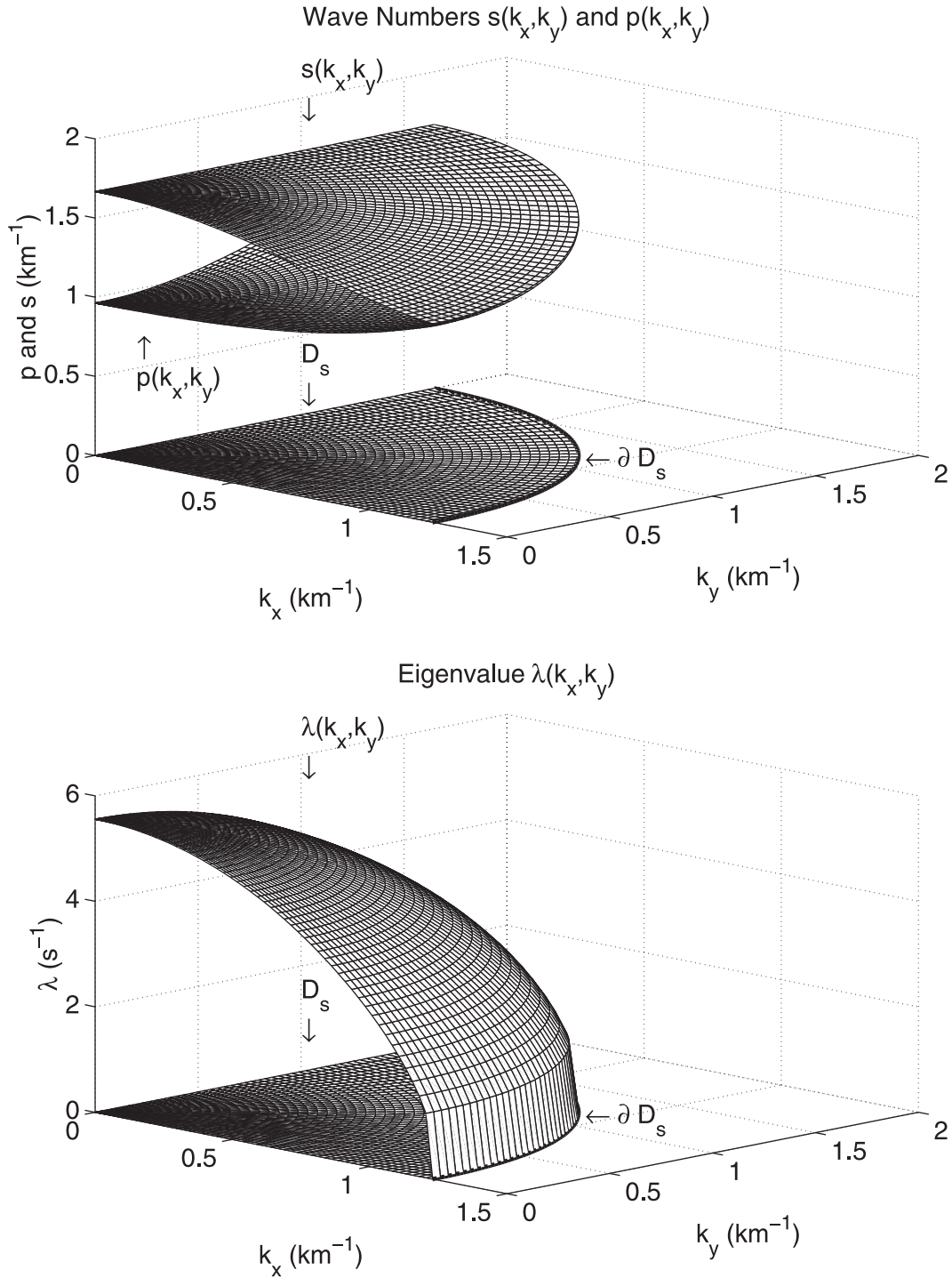
Wave Numbers $s(k_x,k_y)$ and $p(k_x,k_y)$

Eigenvalue $\lambda(k_x,k_y)$

Figure 4. Eigenvalue analysis. In the $x - y$ Fourier domain we show the spectral domain and the numerical solution for the waves numbers, p and s, of the Helmoltz potentials and the corresponding eigenvalue λ. Numerical values are $\rho = 3000 \text{kgm}^{-3}$, $v_s = 3333 \text{ms}^{-1}$, $\eta = v_p/v_s = \sqrt{3}$, $\sigma_s - \sigma_d = 10 \text{MPa}$, and $L_c = 0.18 \text{m}$.

$= -\sigma_{zz}^\infty \mu_s$ at $t = 0$. We put a perturbation in this system and observe the growth of the slip on the fault. We simulate the evolution by a finite-difference computation. We take $L_c = 0.18$ m and therefore $\alpha_c = 0.0017$ m^{-1}.

[9] In Figure 3 we present the different phases of the process. The slip evolution can be divided into three successive phases: wave, initiation, and crack. The wave

phase ($0s < t < 0.4$ s) is associated with the propagation of the perturbation on the fault. It is not of interest because its amplitude remains of the order of the perturbation. The initiation phase ($0.4s < t < 3$ s) prepares the rupture. It is the progressive fracturing process appearing before the rupture propagation. As we will see further, this phase is dominated by unstable modes, but it does not radiate

waves. The crack phase ($t > 3$ s) begins when some points on the fault have overcome the critical slip $2L_c$. It corresponds to the rupture propagation and the radiation of the strong motion.

[10] In this section our aim is to extract the 3-D spectral properties of the initiation phase on the infinite fault. The method is derived from the one that we used previously in the corresponding 2-D in-plane problem [see *Favreau et al.*, 1999]. We develop the spectral analysis under the condition that all of the fault remains in the weakening part of the friction law, i.e., $0 \le \delta u_x(t, x, y) \le 2L_c$. We also assume that unloading will not happen. Consequently, the frictional condition at any point of the fault is

$$\frac{\sigma_{xz}(t,x,y,0)}{\rho v_s^2} = -\alpha_c u_x(t,x,y,0^+). \qquad (16)$$

Since the problem is now linearized, we can perform a spectral representation of the solution on a basis of eigenmodes. We will especially look for the unstable modes, the ones that give the growing part of the solution, also called the dominant part.

3.1. The Spectral Problem

[11] The spectral problem is given in Appendix A. The eigenvalue is denoted λ, and the eigenfunctions are denoted $\Phi^\lambda(x, y, z)$ and $\Psi_i^\lambda(x, y, z)$, $i = (x, y, z)$. In general, to extract the growing part in the spectral representation of a solution, one has to find the eigenvalues whose real part is positive ($Re(\lambda) > 0$). In our case, where elastodynamics are coupled with a slip-dependent friction law, there are simplifications. First, if λ is a solution, $-\lambda$ is one too. Second, we have $\lambda^2 \in \Re$. This can be shown in 3 dimensions in the manner of *Favreau et al.* [1999] for the 2-D in-plane case. Consequently, $\lambda \in \Re$ or $\lambda \in \Re$. For $\lambda \in \Re$ the eigenmodes are oscillating in time and represent the part of the solution with stable or decreasing amplitude (wave part). If $\lambda \in \Re$, the eigenmodes are growing exponentially in time and describe the unstable part of the solution that is dominant after sufficiently large times. In the same way as *Favreau et al.* [1999], these growing modes can be found in the following set of plane-wave solutions:

$$\Phi^\lambda(x,y,z) = e^{ik_x x + ik_y y - pz} \qquad (17)$$

$$\Psi_i^\lambda(x,y,z) = S_i e^{ik_x x + ik_y y - sz}, i = (x,y,z) \qquad (18)$$

$$s \in \Re^+, s \ge \sqrt{k_x^2 + k_y^2} \qquad (19)$$

$$p \in \Re^+, p = \frac{1}{\eta}\sqrt{(\eta^2 - 1)(k_x^2 + k_y^2) + s^2} \qquad (20)$$

$$\lambda \in \Re, \lambda = \pm v_s \sqrt{s^2 - k_x^2 - k_y^2}, \qquad (21)$$

where $(k_x, k_y) \in \Re^2$ are the Fourier wave numbers corresponding to the space variables (x, y). $1/p$ and $1/s$ represent the penetration lengths in the exponential decay of the potentials.

[12] In Appendix A we solve analytically the expressions of the amplitudes S_i, $i = (x, y, z)$ in equation (18), and we

derive a condition on the wave numbers k_x and k_y that defines the spectral domain

$$D_s : \frac{k_x^2}{k_{xc}\sqrt{k_x^2 + k_y^2}} + \frac{k_y^2}{k_{yc}\sqrt{k_x^2 + k_y^2}} \le 1, k_{xc} = \frac{\alpha_c}{\gamma}, k_{yc} = \alpha_c,$$
$$\gamma = 2(1 - 1/\eta^2). \qquad (22)$$

We remark that k_{xc} and k_{yc} are the spectral cut-cutoffs of the 2-D in-plane and antiplane problems found in the studies by *Campillo and Ionescu* [1997] and *Favreau et al.* [1999]. By ∂D_s, we denote the contour of D_s. For each point (k_x, k_y) of D_s defined by equation (22), we find numerically the wave numbers $s(k_x, k_y)$ and $p(k_x, k_y)$ and the associated eigenvalue $\lambda(k_x, k_y)$. In Figure 4 (top) we represent the numerical solution of $p(k_x, k_y)$ and $s(k_x, k_y)$ on D_s in the quarter ($k_x \ge 0$, $k_y \ge 0$). In Figure 4 (bottom) we plot $\lambda(k_x, k_y)$. We remark that for $k_x = k_y = 0$ we have $s(0, 0) = \alpha_c$, $p(0, 0) = \alpha_c/\eta$ and we have the largest real eigenvalue $\lambda(0, 0) = v_s\alpha_c$. On ∂D_s, we have $s(\partial D_s) = p(\partial D_s) = \sqrt{k_x^2 + k_y^2}$ and $\lambda(\partial D_s) = 0$. In the following sections the functions s, p, and λ are considered as known functions of the wave numbers k_x and k_y.

3.2. The Dominant Part and Its Validation

[13] The details of the following analysis are given in Appendices B and C. The dominant part of the displacement field can be constructed on the basis of the eigenfunctions corresponding to real eigenvalues ($\lambda \in \Re$). It is written as

$$u_i^d(t,x,y,z) = \int \int_{D_s} u_i^{k_x,k_y}(z)e^{i(k_x x + k_y y)}$$
$$\cdot \left(W_0(k_x, k_y)\cosh(\lambda t) + \frac{W_1(k_x, k_y)}{\lambda}\sinh(\lambda t) \right)dk_x dk_y, \qquad (23)$$

where functions $u_i^{k_x,k_y}(z)$ are derived from the z dependence of the eigenfunctions (see Appendix B). The weights $W_0(k_x, k_y)$ in formula (23) are calculated from the spatial Fourier transform in (x, y) of the initial conditions in displacement $\tilde{u}_i^0(k_x, k_y, z)$ (see Appendix B). Let us use the notation $(\ldots)^\star$ for the conjugate complex. We find for the weights $W_0(k_x, k_y)$,

$$W_0(k_x \cdot k_y) = \frac{1}{N(k_x, k_y)}\int_0^{+\infty}\sum_{i=x,y,z}\left((u_i^{k_x,k_y})^*(z)\tilde{u}_i^0(k_x,k_y,z)\right)dz, \qquad (24)$$

where $N(k_x, k_y)$ is the norm of the eigenfunctions calculated in Appendix B. The coefficients $W_1(k_x, k_y)$ are calculated by taking the spatial Fourier transform in (x,y) of the initial conditions in velocity $\tilde{v}_i^0(k_x, k_y, z)$.

[14] To compare the solution (23) with a finite-difference simulation, we use a narrow Gaussian perturbation of half-width a, i.e., $v_x^0(k,y,z) = v_0 e^{-(x^2+y^2+z^2)/a^2}$. The analytical expression of $W_1(k_x, k_y)$ for this shape of perturbation is given in Appendix C. The finite-difference algorithm is based on an adaptation of the one used and described by *Ionescu and Campillo* [1999]. The scheme is explicit. We use operator splitting for the bulk and integration along
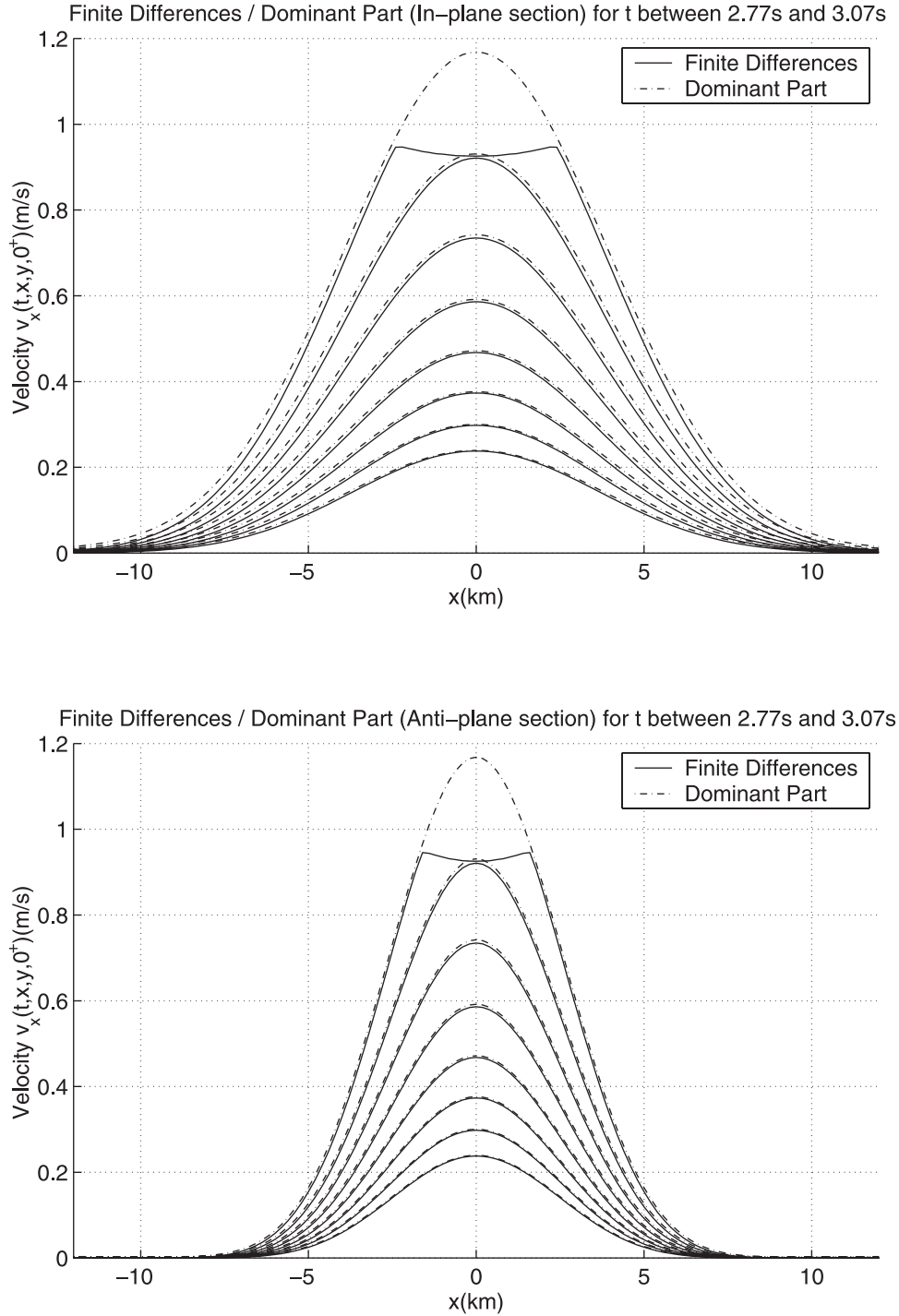
Finite Differences / Dominant Part (In–plane section) for t between 2.77s and 3.07s

Finite Differences / Dominant Part (Anti–plane section) for t between 2.77s and 3.07s

Figure 5. Numerical test of the dominant part. The slip velocity on the fault is presented in two sections along x (in-plane) and along y (antiplane). Numerical values are $\rho = 3000 kgm^{-3}$, $v_s = 3333 ms^{-1}$, $\eta = v_p/v_s = \sqrt{3}$, $\sigma_s - \sigma_d = 10MPa$, and $L_c = 0.18m$.

characteristics for the boundary condition. The method was tested in antiplane [see *Ionescu and Campillo*, 1999] and in-plane [see *Favreau et al.*, 1999] cases. In Figure 5 we compare the two solutions to determine the accuracy of our analysis. We plot the complete solution computed by the finite-difference method and the analytical dominant part on the fault. The grid used in the finite-difference computation is $480 \times 480 \times 240$. The analytical dominant part is a good approximation of the initiation process. In the sets of simulations that we performed the misfit at the center of the fault does not exceed a few percent. This misfit can be considered as good enough since we compare two exponential evolutions (therefore the difference of slip velocity between two consecutive time steps is huge). This tends to dramatically amplify the effect of the initial conditions. The dominant part can be evaluated at any desired accuracy, but
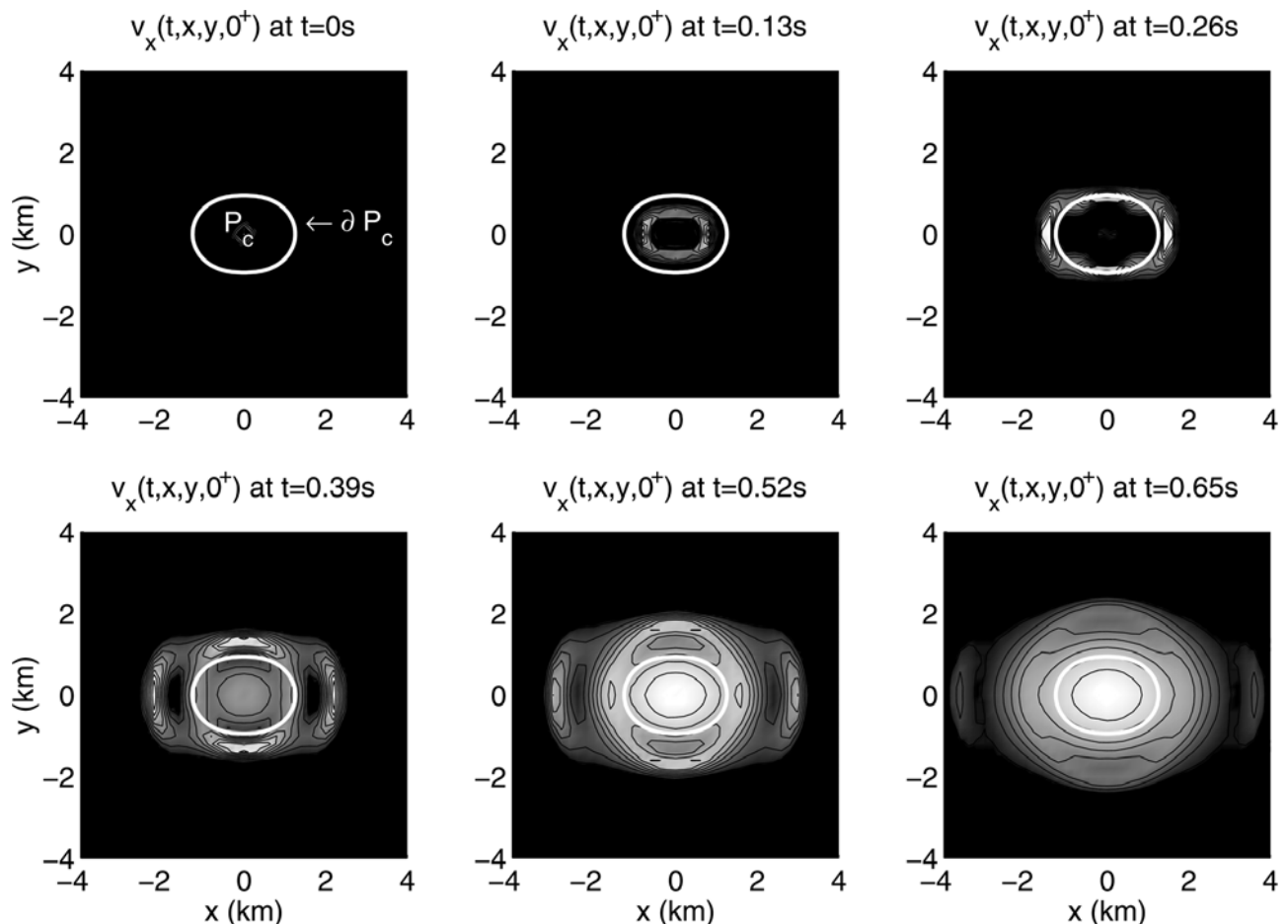
Figure 6. The complete slip velocity distribution (white pattern), simulated by finite-difference computation for the locally perturbated infinite fault. To have a clearer image, we superpose a few contour lines (thin black lines). The slipping patch P_c, contoured by the white line (∂P_c), represents the characteristic area needed to see the dominance of the unstable modes in the slip evolution on an infinite fault. This dominance appears clearly at $t = 0.52$s. Numerical values are $\rho = 3000$kgm^{-3}, $v_s = 3333$ms^{-1}, $\eta = v_p/v_s = \sqrt{3}$, $\sigma_s - \sigma_d = 10$MPa, and $L_c = 0.18$m.

in the finite-difference computation an error can appear just by the way the initial condition is implemented. Far from the center of the fault the error becomes important. The main reason is that the dominant part is a noncausal approximation of the complete solution. This situation has been already encountered and discussed by *Campillo and Ionescu* [1997] and *Favreau et al.* [1999] when extracting a single mode or a subset of modes among the complete set that constitute the solution. *Knopoff et al.* [2000] discuss that point in more detail by searching an analytical expression of the entire solution in the 2-D antiplane case for a concentrated perturbation on the fault. Ampuero et al. (J.-P. Ampuero et al., Nucleation of rupture under slip-dependent friction law: Simple models of fault zone, submitted to *Journal of Geophysical Research*, 2001, hereinafter referred to as Ampuero et al., submitted manuscript, 2001) found a causal Green's function for the slip-weakening antiplane problem. The solution found by *Knopoff et al.* [2000] and Ampuero et al. (submitted manuscript, 2001) is causal on the fault because it has a more extended spectral content than the dominant part. However, as we show in this study and in our earlier works, the shape of the slip and the

dynamic properties of the system are very well approximated by the noncausal dominant part. Indeed, it correctly fits the complete solution, as simulated by finite-difference computation. Finally, let us remark that at a later stage the slip velocity saturates at the center of the fault because the slip has overcome the critical slip. Indeed, the crack propagation regime begins. The slip-weakening process is bounded in a remaining breakdown zone. *Favreau et al.* [1999] have shown that the dominant part can be a reasonable approximation of the slip process in the breakdown zone. Here we do not know if this property is true.

3.3. Essential Properties Inferred by Spectral Analysis

[15] Some details of the following analysis are given in Appendix D. The slip is governed by the dominant part, which is a solution based on a continuous and bounded spectral domain D_s. The spectral cut-off governs the shape of the growing slip zone due to a concentrated perturbation. The existence of this specific pattern leads us to introduce the concept of slipping patch P_c. We must warn the reader that the definition of the slipping patch introduced here is subjective, but it is justified later on. First, let us recall that, in the spectral

domain, the definition of D_s has no ambiguity. The following definition for the slipping patch P_c is more physical than mathematical, but it is simple and natural. For each direction θ in the spectral domain, condition (22) implies a spectral cut-off at the critical spectral radius $k_c(\theta) = \frac{\alpha_c}{\gamma \cos^2 \theta + \sin^2 \theta}$. To this critical spectral radius we associate the corresponding critical length $l_c(\theta) = \frac{\pi}{k_c(\theta)} = \frac{\pi}{\alpha_c} (\gamma \cos^2 \theta + \sin^2 \theta)$. Then we define the slipping patch by the following fault domain (we note that $r = \sqrt{x^2 + y^2}$).

$$P_c : r \leq \frac{l_c(\theta)}{2} \Longleftrightarrow \left(\sqrt{x^2 + y^2} \right)^3 \leq \frac{l_{xc}}{2} x^2 + \frac{l_{yc}}{2} y^2, \; l_{xc} = \frac{\pi \gamma}{\alpha_c},$$
$$l_{yc} = \frac{\pi}{\alpha_c}. \tag{25}$$

To show the physical meaning of the slipping patch P_c defined by equation (25), we plot in Figure 6 the distribution and the contour of the complete slip velocity solution on the fault (finite-difference computation) at the beginning of the slip process. The white line is ∂P_c, the contour of P_c. At the beginning ($t < 0.26$ s) we see a propagating pulse that corresponds to the propagation of the perturbation. This pulse does not grow. When the perturbation just passes ∂P_c (at $t = 0.26$ s), we begin to see a patch inside the propagative phases of the perturbation. This patch grows until $t = 0.52$ s. The patch is clearly visible at $t = 0.52$ s, when its contour is close to the critical contour ∂P_c. For $t > 0.65$ s all of the propagative phases become less visible and the nonpropagative patch grows exponentially; the evolution is now dominated by the unstable modes. P_c has no clear significance thereafter, but its aspect ratio gives the aspect ratio of the slip velocity distribution in the initiation process. P_c can be interpreted as the typical fault domain through which a concentrated perturbation needs to travel before one sees the dominance of the unstable modes in the slip velocity distribution.

[16] After a certain time the slip process at the center of the perturbation is governed by the most dominant eigenfunction, i.e., the one corresponding to $k_x = k_y = 0$. This eigenfunction is $u_x^{0,0}(z) = \alpha_c^3 e^{-\alpha_c |z|}$ and $u_y^{0,0}(z) = u_z^{0,0}(z) = 0$. Consequently, the slip decays from the fault approximately like $e^{-\alpha_c z}$; the displacement field and the signal are localized around the fault, and the source process can be considered as a nonradiative process. This feature was verified by the finite-difference computation. Furthermore, since this eigenfunction has the eigenvalue $\lambda(0,0) = v_s \alpha_c$, the slip velocity grows in time approximately like $e^{v_s \alpha_c t}$. We can therefore give a theoretical approximation of the time of initiation T_c at which the critical slip $2L_c$ is reached at the center of the perturbation. For a narrow perturbation of half-width a and under the conditions $a \ll \pi/\alpha_c$ and $T_c \gg 1/(\alpha_c v_s)$, we obtain (see Appendix D)

$$T_c = \frac{1}{\alpha_c v_s} \ln \left(\frac{L_c}{\frac{\pi \alpha_c^5 (\gamma+1)}{12 \gamma^{3/2}} \left(W_0(0,0) + \frac{W_1(0,0)}{v_s \alpha_c} \right)} \right). \tag{26}$$

The value of T_c found by equation (26) in Appendix D is 2.81s, whereas it is 3.00s in the finite-difference computation. The small misfit comes from our approximation (equation (26)), where the slip evolution is approximated by $e^{v_s \alpha_c t}$. Note that this corresponds to the infinite wavelength approximation of the elastodynamic 2-D and 3-D kernels given by a 1-D expression $\sigma_{xz} - \sigma_{xz}^\infty = -(\rho v_s/2) \, \delta v_x$ (see Ampuero et al., submitted manuscript, 2001). This approximation is not true at the beginning of the process, when contributions of all the dense spectral domain D_s participate in the solution. A higher order estimate could be calculated by taking the contribution of a neighborhood of modes enclosing the fastest one.

4. Finite Fault Model

[17] The time of initiation T_c of an infinite fault depends essentially on the maximum eigenvalue $\lambda = v_s \alpha_c$. The corresponding numerical value of T_c is small for the homogeneous infinite fault (a few seconds at most), assuming reasonable physical parameters. As shown by *Ionescu and Campillo* [1999] and *Dascalu et al.* [2000] for the 2-D antiplane case, the time of initiation can be much longer for finite faults, depending on the size of the fault. More details on the 2-D problems are given in Appendix E. Since a complete analytical study of the finiteness effect in 3-D is not complete at present, we limit our analysis to the main features exhibited by a canonical example.

[18] The finite fault is defined by a homogeneous slip-weakening zone bounded by a barrier of infinite strength, and consequently, the slip is null outside the fault. The infinite strength of the barriers implies a singular stress field at the edge of the fault. Although this is physically not admissible, a recent work by Uenishi et al. (K. Uenishi et al., Nucleation length for slip-weakening rupture instability under nonuniform fault loading, submitted to *Journal of Geophysical Research*, 2001, hereinafter referred to as Uenishi et al., submitted manuscript) confirms that an antiplane fault progressively loaded under any heterogeneous prestress and having moving barriers to avoid stress singularity bifurcates to instability when it reaches a critical size. This critical size corresponds exactly to the critical size found earlier by *Ionescu and Campillo* [1999] and *Dascalu et al.* [2000] for fixed barriers of infinite strength. The more mechanical approach of Uenishi et al. (submitted manuscript, 2001) confirms and justifies the purely geometrical nature, "the finiteness effect," of the nucleation length found by *Dascalu et al.* [2000]. In consequence, by choosing barriers of infinite strength, we follow the pure geometrical approach. For the shape of the finite fault we choose a canonical case, where the fault is self-similar to the slipping patch P_c defined in section 3. This particular choice is interesting because it corresponds to the case where the finiteness effect has equal influence in every direction of the fault plane. We denote the factor of self-similarity ζ, which is a ratio of length. For $\zeta = 1$ the finite fault is identical to the slipping patch P_c, and for $\zeta = +\infty$ the fault is infinite. We call such a fault a "canonical finite fault."

4.1. Domain of Stability of the Canonical Finite Fault

[19] Here we determine numerically the condition of stability of the canonical finite fault. We search the critical value of ζ, denoted ζ_0, under which the faults are stable and over which they are unstable. In practice, we fixed the size
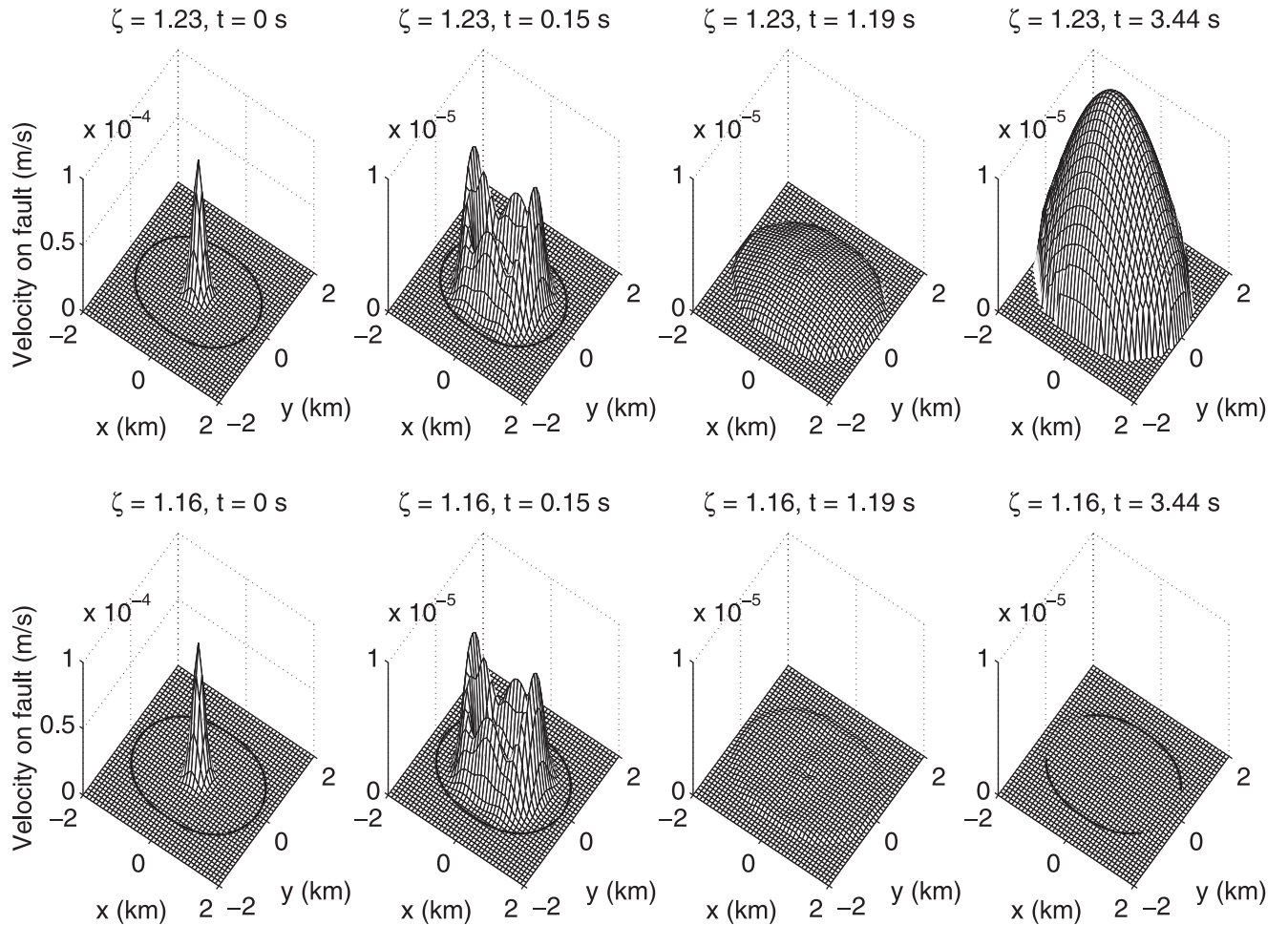
Figure 7. Here is the numerical detection of the critical point for the canonical faults, whose shape is self-similar to the slipping patch P_c. Parameter ζ is the length scaling factor of the fault compared to the slipping patch P_c. The faults with $\zeta > 1.23$ are unstable, while the ones with $\zeta < 1.16$ are stable.

of the canonical fault, and we modified the size of the slipping patch P_c by changing the critical slip $2L_c$. We performed a series of finite-difference triggering experiments for a wide range of ζ, and we approached the critical point ζ_0 step by step. In Figure 7 we present the two numerical experiments that surround the critical point. We plot the velocity on the fault for two close sizes of slipping patches P_c (P_c is the black solid line). In the case $\zeta = 1.23$ (top) the fault is unstable because the slip grows after the perturbation. In the case $\zeta = 1.16$ (bottom) the fault is stable and the perturbation vanishes. This confirms that the set of canonical faults admits a point of transition ζ_0 that delimits the stable and the unstable domains. The precise calculation of this point is difficult with the finite-difference method, but we can give $\zeta_0 \approx 1.2 \pm 0.05$. For a 2-D antiplane finite fault of length $2a$ we found a theoretical and numerical point of transition such that $a\alpha_c = 1.15777\ldots$, which corresponds to $\zeta_0 = 0.7370\ldots$. In Appendix E it is shown that this last value of ζ_0 is the same in 2-D antiplane and in-plane faults. However, the difference between 2-D and 3-D finite faults can be explained by better confining of the slip pattern in the 3-D case. This involves stronger elastic forces acting on the fault and a slip stabilization for larger faults. So in three dimensions the fault needs to be larger than the

slipping patch to be unstable, i.e., $\zeta_0 > 1$, whereas it can be smaller in two dimensions, i.e., $\zeta_0 < 1$.

4.2. The Unstable Behavior of the Canonical Finite Fault

[20] In the following we consider unstable faults, i.e., when $\zeta > \zeta_0$, and concentrate on the rate of instability of the fault. To give meaning to this rate of instability, we must introduce some spectral properties of the finite fault. As we know from 2-D antiplane studies [see *Dascalu et al.*, 2000], the initiation process on an unstable 2-D finite fault can be described by a dominant part that corresponds to the part of the spectrum with eigenvalues of positive square ($\lambda^2 > 0$). Unlike the infinite fault the spectrum of the 2-D unstable finite fault is discrete, and consequently the spectrum of the dominant part is discrete as well. By λ_0 we denote the positive first and largest eigenvalue of the spectrum of the dominant part. The slip evolution is simply $e^{\lambda_0 t}$, and the time of initiation is inversely proportional to the eigenvalue λ_0, which can be called the "rate of instability." We now extend the same properties for a 3-D finite fault. In other words, the initiation process can be described by one single dominant mode. This mode gives the dynamical characteristics of the fault
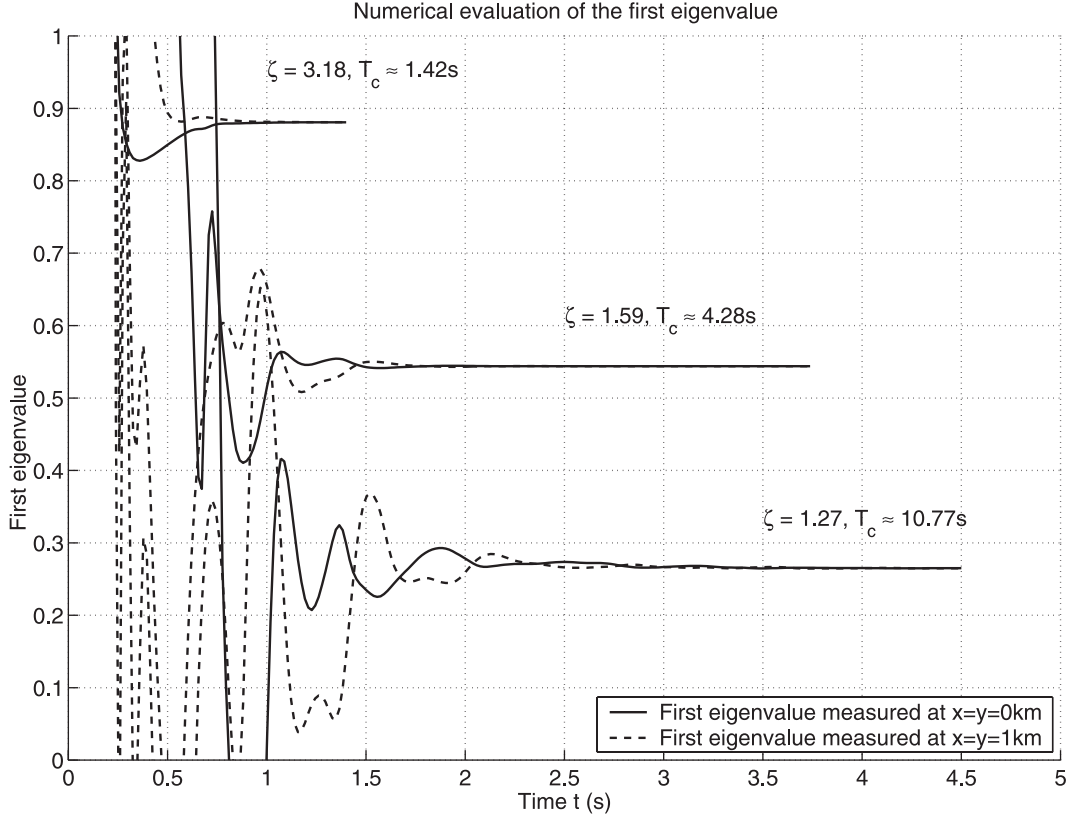
Figure 8. The numerical measure of the first eigenvalue of unstable canonical faults. The first eigenvalue is computed numerically at different points on the fault by computing the dimensionless exponent $\frac{\lambda_0}{v_s \alpha_c} \approx \frac{1}{v_s \alpha_c} \frac{\partial \ln v_x(t,x,y,0^+)}{\partial t}$. Here we show the spatial and temporal stabilization of the exponent that governs the slip on finite faults in the initiation phase. The initial oscillations are due to the perturbation used to trigger the fault. They disappear when the first unstable mode dominates.

independently of the perturbation used to trigger it. Consequently, we concentrate here on the determination of the eigenvalue λ_0 rather than on the time of initiation. To this end we show numerically that the slip on the canonical fault is governed by an exponential growth. The exponent of the slip growth is considered as identical to the eigenvalue λ_0. The procedure is the following: we run finite-difference triggering experiments and we vary the dimension of the slipping patch P_c by changing the critical slip $2L_c$. For each simulation we plot an estimation of the dimensionless eigenvalue $\lambda_0/(v_s \alpha_c)$ (see Figure 8). For a given perturbation the quantity $\lambda_0(\zeta)/(v_s \alpha_c)$ is strongly related to the inverse of the number of shear wave travels performed inside the fault during the initiation process. The value of $\lambda_0/(v_s \alpha_c)$ is estimated using

$$\frac{\lambda_0}{v_s \alpha_c} \approx \frac{1}{v_s \alpha_c} \frac{\partial \ln v_x(t,x,y,0^+)}{\partial t}. \quad (27)$$

This quantity is shown in Figure 8; it remains constant in time and space once the instability develops. This confirms that the slip is rapidly governed by a single mode during the initiation process. This shows that when finiteness is present, unstable modes are well separated (the spectrum is not dense), as *Dascalu et al.* [2000] show theoretically in the 2-D antiplane case.

[21] In Figure 9 we plot $\lambda_0/(v_s \alpha_c)$ for a wide range of fault dimensions by varying ζ. In practice, the finite-difference calculation was difficult for $\lambda_0/(v_s \alpha_c) < 0.1$ because small values of the eigenvalue imply a long initiation duration. Note the sharp slope at $\zeta = \zeta_0$, which shows the strong sensitivity of the rate of instability at the beginning of the unstable domain. This implies that a small change in the fault parameters has a significant impact on its rate of instability. In the 2-D antiplane case, *Dascalu et al.* [2000] show theoretically that the slope at the critical point is vertical (see also Appendix E and Figure 9). Since the structure of the spectral problem of the 3-D canonical finite fault should be similar to the one of the 2-D finite fault, we speculate that its slope is also vertical. Furthermore, since the physical problem is of order 2 in time, we can expect a behavior like $\lambda_0/(v_s \alpha_c) \sim A(\zeta - \zeta_0)^{\frac{1}{2}}$, $A > 0$ at the critical point, as shown by Ampuero et al. (submitted manuscript, 2001) in the 2-D antiplane case.

4.3. The Unstable Behavior of Other Faults With Other Geometries

[22] We propose to look at the influence of other transformations of the fault on its rate of instability. For this we consider a change of geometry that consists of stretching the fault shape in one direction (i.e., we change the ellipticity of
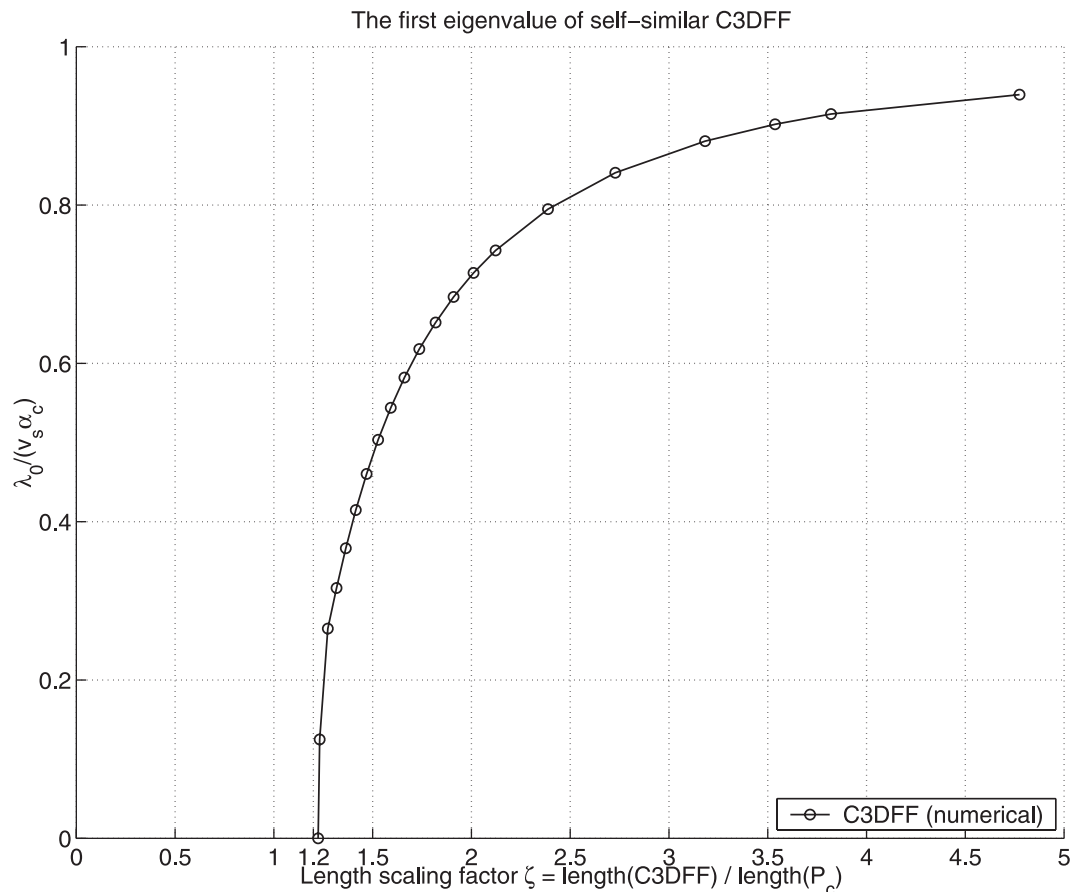
Figure 9. The first eigenvalue for the canonical faults. The eigenvalue admits a sharp slope at the critical point ($\zeta = 1.2$). For $\zeta \to \infty$, it tends to the value predicted by the infinite fault analysis, i.e., $\frac{\lambda_0}{v_s \alpha_c} \to 1$.

the fault). We consider three fault families: (1) the critical canonical shape stretched in the in-plane direction, (2) the critical canonical shape stretched in the antiplane direction, and (3) the self-similar increase of the surface, as described in section 4.2. To compare the three experiments, we show their estimated first eigenvalues as a function of the increasing surface ratio χ in Figure 10. For (1) and (2) we perform new sets of computations by changing the ellipticity of the fault. For (3) we simply operate the variable change $\chi = (\zeta/\zeta_0)^2$ in presenting the results of the experiments performed in the previous paragraph. Although artificial, this new change of variable allows us to plot the results of experiments (1), (2), and (3) in the same frame. When $\chi = 1$, all faults in experiments (1), (2), and (3) are identical to the critical canonical fault. We must note that in experiment (3) the change of abscissa ζ into abscissa χ does not affect the type of slope exhibited by the eigenvalue λ_0 at the critical point.

[23] Figure 10 shows several features. First, faults stretched in the antiplane or in the in-plane direction have similar first eigenvalues. This means that the canonical fault exhibits an isotropic behavior due to its special aspect ratio and shape. In other words, the canonical fault shows the same change in its unstable behavior for different stretching direction. Second, they both have an asymptote (around 0.7) that corresponds logically to the exponent of an unstable

2-D finite fault at $\zeta = 1.2$. (see Figure 9 and Appendix E). This result, though trivial, means that a 3-D evolving fault can maintain a much lower rate of instability than $v_s \alpha_c$ for a long period of time. Indeed, if we assume that the fault geometry evolves by a stretching process into a 2-D fault geometry, the fault can remain weakly unstable. In the stretching case studied here the rate of instability tends to about 0.7, but this final rate could have been lower. For example, compared with the canonical fault, a narrower fault in the antiplane geometry stretched in the in-plane direction will become less unstable since its final rate of instability will correspond to the one of a narrow antiplane fault. We could also consider an extreme case where one stretches (in the in-plane direction) a very narrow fault (in the antiplane direction), such that it will never become unstable. Third, in the stretching experiments (1) and (2), the curves seem to exhibit a quasi-vertical slope at $\chi = 1$ as in experiment (3). This means that in general, for finite faults close to their limit of stability, the rate of instability is not only very sensitive to their size but also to their geometry. This third remark is not in contradiction with the second one; nevertheless, it shows the limit of our geometrical approach. Will the canonical shape or a narrower shape be favored in nucleation processes? If one assumes that the barriers break naturally, the canonical shape being more unstable
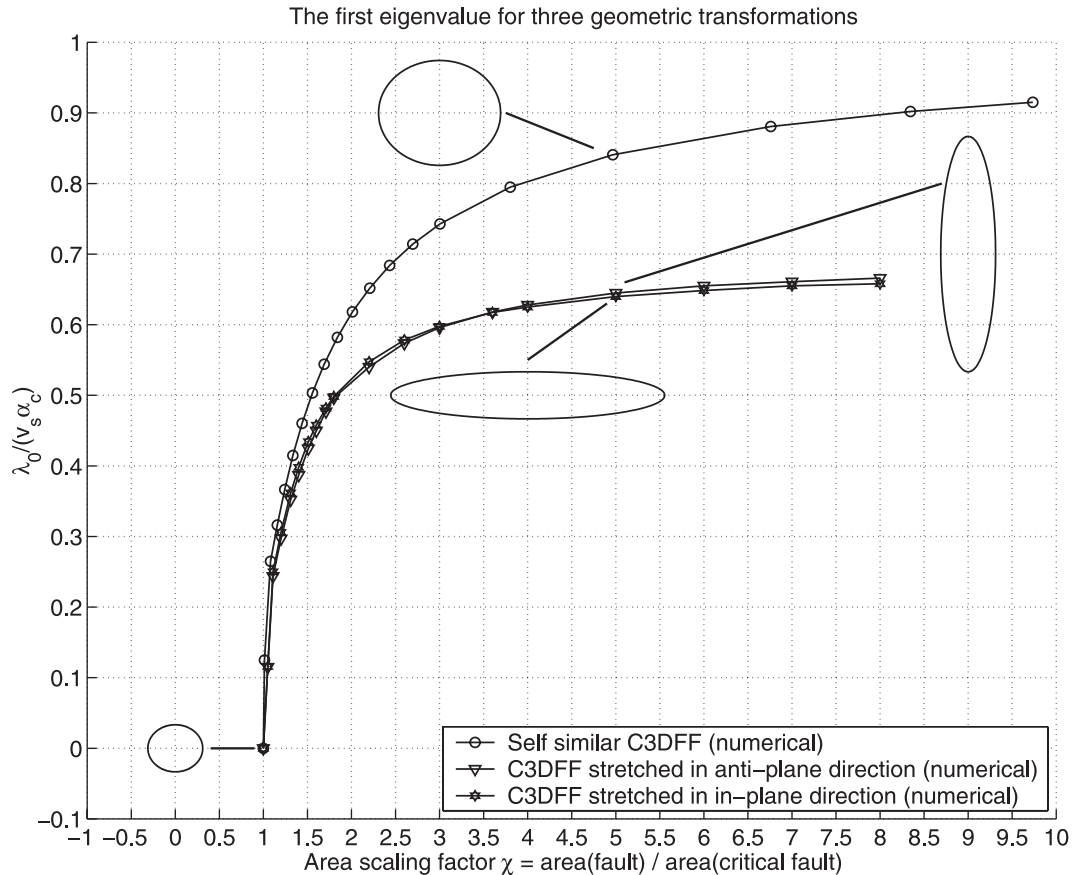
Figure 10. The first eigenvalue for other types of fault geometry. Here we show the evolution of the rate of instability by changing the shape of the critical canonical fault in three different manners. Here χ represents the scaling factor of the fault areas versus the area of the critical canonical fault. In every case we note the sharp transition of the rate of instability at the critical point.

for a given surface, it can probably be the preponderant mode of fault patch growing.

5. Conclusion

[24] We define a three-dimensional model of unstable dynamic initiation where the crust is modeled by an elastodynamic body and the fault is modeled by a flat interface subject to a slip-weakening friction law. We perform a spectral study of the free initiation process on an infinite fault. We find the spectral domain on which the slip instability develops, and we derive a method to calculate the dominant part of the slip solution. The physical properties of this free slip process can be summarized by three points. First, the shape of the growing slip is given by a pseudoelliptical slipping patch P_c that scales with the inverse of the rate of weakening α_c. Second, it decays exponentially in the bulk with the penetration depth $1/\alpha_c$. Third, it grows exponentially with the characteristic time $1/(v_s\alpha_c)$.

[25] We introduce the finiteness effect of the slipping zone. The slipping zone can be either an entire fault or a nucleation zone. We show the transition between the stable and the unstable domain for a particular set of canonical faults, which are self-similar to the slipping patch P_c. When the fault is unstable, we show numerically that the slip

evolves on one single eigenmode. Its eigenvalue λ_0 gives the characteristic time of initiation through its inverse.

[26] Interesting features appear in this study. First, at the critical point the rate of instability is very sensitive to the size and the geometry of the slipping zone. However, other models do not predict this sharp transition. In our model the timescale of the initiation process is given by the elastodynamic interaction of the body combined with the slip-weakening behavior of the interface. A modification in the model of either the behavior of the body or the behavior of the interface can lead to a very different qualitative behavior concerning the duration of the initiation. For example, the introduction of timescales like viscosity in the friction law can dominate by their smoothing effect on the transition. This is the case of rate-and-state friction laws. In the same way, simplifications of the elastodynamic properties such as the quasi-dynamic approximation can smooth the transition. The type of transition at the critical point is therefore an important factor in initiation since the duration of the initiation and the time to detect the associated deformation depends on it. Second, it is possible to imagine a long initiation process coupled with an evolution of the slipping zone. This requires that the domain extends mainly in one direction. This situation can be encountered in a stratified structure. However, in most cases, the model tends to predict a rapid evolution of a fault system around

its critical point. This specific behavior may be of interest in understanding earthquake triggering and fault instability. In triggering phenomena our model has been used in a 2-D antiplane geometry by *Voisin et al.* [2000] to infer the frictional properties (α_c and L_c) of the second fault segment involved in the 1980 Irpinia earthquake. In their study of slow initial phases, *Shibazaki and Matsu'ura* [1998] show with a 2-D antiplane model that realistic signals can be computed by assuming scaling relations between laboratory stick-slip experiments and natural earthquakes. Helped by the present work, these studies could be generalized in a 3-D elastodynamic framework, especially the computation of the 3-D radiation of slow initial phases.

[27]   To conclude, the model predicts that the precursory deformation caused around the fault by the initiation process should be synchronized with a low amplitude and an exponential increase in time. Therefore this precursory deformation is at the junction between geodetic and seismologic measurements.

Appendix A: The Eigenvalue Problem of the Infinite Fault

[28]   The problem being linearized, eigenfunctions $\Phi^\lambda(x, y, z)$, $\Psi_i^\lambda(x, y, z)$, $i = (x, y, z)$ verify for all $z > 0$,

$$\lambda^2 \Phi^\lambda = v_p^2 \nabla^2 \Phi^\lambda, \quad \lambda^2 \Psi_i^\lambda = v_s^2 \nabla^2 \Psi_i^\lambda, \ i = (x, y, z) \tag{A1}$$

$$\frac{\partial \Psi_x^\lambda}{\partial x} + \frac{\partial \Psi_y^\lambda}{\partial y} + \frac{\partial \Psi_z^\lambda}{\partial z} = 0. \tag{A2}$$

On the fault at $z = 0$ they verify

$$(\eta^2 - 2)\left(\frac{\partial^2 \Phi^\lambda}{\partial x^2} + \frac{\partial^2 \Phi^\lambda}{\partial y^2} + \frac{\partial^2 \Phi^\lambda}{\partial z^2}\right) + 2\left(\frac{\partial^2 \Phi^\lambda}{\partial z^2} + \frac{\partial^2 \Psi_y^\lambda}{\partial x \partial z} - \frac{\partial^2 \Psi_x^\lambda}{\partial y \partial z}\right) = 0 \tag{A3}$$

$$\frac{\partial \Phi^\lambda}{\partial y} + \frac{\partial \Psi_x^\lambda}{\partial z} - \frac{\partial \Psi_z^\lambda}{\partial x} = 0 \tag{A4}$$

$$2\frac{\partial^2 \Phi^\lambda}{\partial x \partial z} + \frac{\partial^2 \Psi_z^\lambda}{\partial y \partial z} - \frac{\partial^2 \Psi_x^\lambda}{\partial x \partial y} + \frac{\partial^2 \Psi_y^\lambda}{\partial x^2} - \frac{\partial^2 \Psi_y^\lambda}{\partial z^2}$$

$$= -\alpha_c \left(\frac{\partial \Phi^\lambda}{\partial x} + \frac{\partial \Psi_z^\lambda}{\partial y} - \frac{\partial \Psi_y^\lambda}{\partial z}\right). \tag{A5}$$

We only search the eigenvalues whose real part is positive ($Re(\lambda) > 0$). Let us recall some results obtained in the context of the in-plane problem [see *Favreau et al.*, 1999] that are also valid in the 3-D problem. First, if λ is a solution, $-\lambda$ is as well (trivial). Second, all eigenvalues have a real square ($\lambda^2 \in \Re$), and consequently λ is imaginary ($\lambda \in \Re$) or real ($\lambda \in \Re$). Consequently, to find the unstable eigenmodes with $Re(\lambda) > 0$, it is equivalent to searching the real eigenvalues ($\lambda \in \Re$). Furthermore, the unstable eigenmodes have to be searched in the following set of plane waves:

$$\Phi^\lambda(x, y, z) = e^{ik_x x + ik_y y - pz} \tag{A6}$$

$$\Psi_i^\lambda(x, y, z) = S_i e^{ik_x x + ik_y y - sz}, \ i = (x, y, z) \tag{A7}$$

$$s \in \Re^+, \ s \geq \sqrt{k_x^2 + k_y^2} \tag{A8}$$

$$p \in \Re^+, p = \frac{1}{\eta}\sqrt{(\eta^2 - 1)(k_x^2 + k_y^2) + s^2} \tag{A9}$$

$$\lambda \in \Re, \lambda = \pm v_s \sqrt{s^2 - k_x^2 - k_y^2}, \tag{A10}$$

where $(k_x, k_y) \in \Re^2$ represents the wave numbers of the displacement field in the $x-y$ Fourier domain. The plane waves of this set verify the wave equations (A1) and the finite energy principle since the displacement is bounded at $z = +\infty$. Equation (A8) is the condition to find $\lambda \in \Re$. Inserting equations (A6) and (A7) in equations (A2), (A3), (A4), and (A5) leads to

$$iS_x k_x + iS_y k_y = S_z s, \ k_x^2 + k_y^2 + s^2$$

$$= 2is(S_y k_x - S_x k_y), \ i(k_y - S_z k_x), = S_x s \tag{A11}$$

$$-2ik_x p - iS_z k_y s - S_y(s^2 + k_x^2) + S_x k_y k_x = -\alpha_c(ik_x + iS_z k_y + S_y s). \tag{A12}$$

By solving the system of linear equations (A11), we deduce the amplitude (S_x, S_y, S_z) of the components (Ψ_x, Ψ_y, Ψ_z):

$$S_x = \frac{ik_y}{2s}, \ S_y \frac{k_x^4 - s^4 + k_y^2(k_x^2 + s^2)}{2isk_x(k_x^2 + k_y^2 - s^2)}, \ S_z = \frac{k_y}{2k_x} \tag{A13}$$

Replacing the amplitudes (A13) in the linearized frictional condition (A12), we have

$$p = \frac{(s^2 + k_x^2)^2 - k_y^2(s^2 - k_x^2) + s\alpha_c(k_x^2 + k_y^2 - s^2)}{4k_x^2 s}. \tag{A14}$$

Finally, a solution of the eigenvalue problem must satisfy both equations (A9) and (A14). By using the polar coordinates (k, θ) such that $(k_x = k\cos\theta, k_y = k\sin\theta)$ and the dimensionless variables $\bar{p} = p/k, (\bar{s}) = s/k$ and $\bar{\alpha}_c = \alpha_c/k$, equations (A9) and (A14) and condition (A8) become

$$\bar{p} = \bar{p}_1(\bar{s}) = \frac{1}{\eta}\sqrt{\eta^2 - 1 + \bar{s}^2} \tag{A15}$$

$$\bar{p} = \bar{p}_2(\bar{s}) = \frac{(\bar{s}^2 + \cos^2\theta)^2 - \sin^2\theta(\bar{s}^2 - \cos^2\theta) - \bar{s}\bar{\alpha}_c(\bar{s}^2 - 1)}{4\bar{s}\cos^2\theta} \tag{A16}$$

$$\bar{s} \geq 1. \tag{A17}$$

For each θ we must find the solutions $\bar{s}$ verifying $\bar{p}_1(\bar{s}) - \bar{p}_2(\bar{s}) = 0$ and $\bar{s} \geq 1$. In Figure A1 we take $\eta = \sqrt{3}$, and we show $\bar{p}_1(\bar{s})$ and $\bar{p}_2(\bar{s})$ for $\theta = 0, \pi/4, \pi/2$ and three different values of $\bar{\alpha}_c$. Note that $\theta = 0$ corresponds to the in-plane mode and $\theta = \pi/2$ corresponds to the antiplane mode. First, $\bar{s} = 1$ is a solution. It corresponds to a null solution. Second, for different $\bar{\alpha}_c$, if the slope of
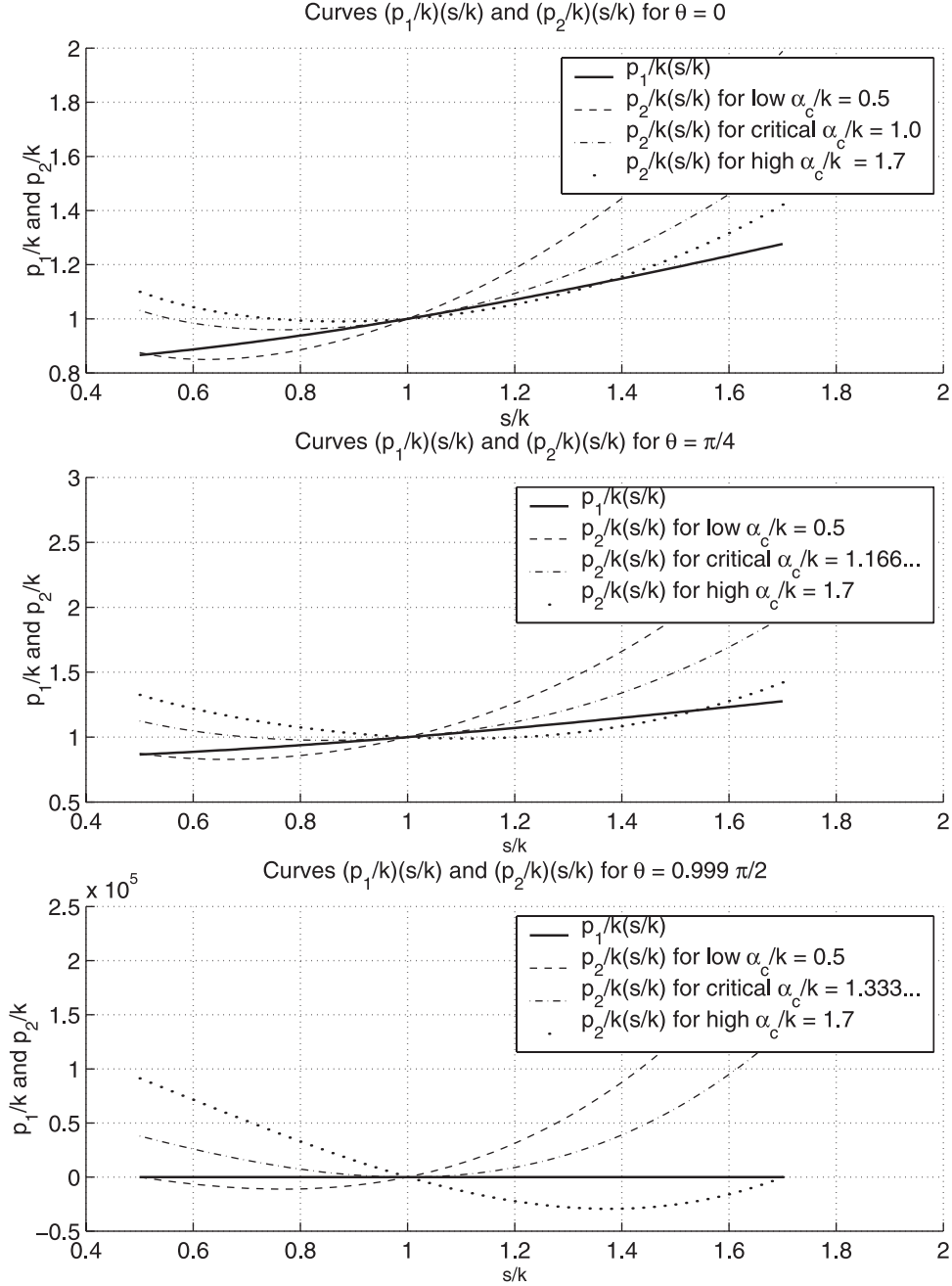
Figure A1. Graphical representation of the dispersion relation $(\bar{p}_1 - \bar{p}_2)(\bar{s})$ that leads to the condition of existence of real eigenvalues. For each direction θ in the spectral domain ($\theta = 0$ corresponds to pure in-plane and $\theta = \pi/2$ to pure antiplane), there exists a critical value of the modulus of the wave number k, such that we can find a nontrivial root s verifying $s > k$ and having real λ. This critical value of k scales with α_c^{-1} and depends also on $\eta = v_p/v_s$. Here $\eta = \sqrt{3}$.

the function $(\bar{p}_1 - \bar{p}_2)(\bar{s})$ at $\bar{s} = 1$ is positive, the function $(\bar{p}_1 - \bar{p}_2)(\bar{s})$ has another nontrivial root $\bar{s} \geq 1$. This can be formulated for each θ as

$$\frac{d(\bar{p}_1 - \bar{p}_2)}{d\bar{s}}(1) \geq 0 \Rightarrow \bar{\alpha}_c \geq \gamma \cos^2 \theta + \sin^2 \theta \;\; \text{with} \;\; \gamma = 2\left(1 - \frac{1}{\eta^2}\right)$$

$$= 2\left(1 - \frac{v_s^2}{v_p^2}\right). \tag{A18}$$

The condition of existence of real eigenvalue (equation (A18)) can be translated into

$$\frac{k_x^2}{k_{xc}\sqrt{k_x^2 + k_y^2}} + \frac{k_y^2}{k_{yc}\sqrt{k_x^2 + k_y^2}} \leq 1, \tag{A19}$$

where $k_{xc} = \frac{\alpha_c}{\gamma}$ and $k_{yc} = \alpha_c$ are the spectral cutoff in the in-plane and in the antiplane directions. We denote the

spectral domain defined by (A19) as D_s, and its contour is denoted ∂D_s.

Appendix B: The Dominant Part for the Infinite Fault

[29] The dominant part is constructed on the basis of eigenfunctions with real λ. Let us define the functions $u_i^{k_x,k_y}(z), i = (x,y,z)$ derived from the z dependence of the eigenfunctions of the potentials (A6) and (A7) by using (A13):

$$u_x^{k_x,k_y}(z) = s(-2k_x^2 e^{-pz} + (s^2 + k_x^2 - k_y^2)e^{-sz}) \quad (B1)$$

$$u_y^{k_x,k_y}(z) = -2sk_xk_y(e^{-pz} - e^{-sz}) \quad (B2)$$

$$u_z^{k_x,k_y}(z) = ik_x(-2pse^{-pz} + (s^2 + k_x^2 + k_y^2)e^{-sz}). \quad (B3)$$

Using these functions, the displacement field associated with the dominant part can be written for $z \geq 0$,

$$u_i^d(t,x,y,z) = \int\int_{D_s} u_i^{k_x,k_y}(z)e^{i(k_xx+k_yy)}$$
$$\cdot \left(W_0(k_x,k_y)\cosh(\lambda t) + \frac{W_1(k_x,k_y)}{\lambda}\sinh(\lambda t)\right)dk_xdk_y, \quad (B4)$$

where weights $W_0(k_x,k_y)$ are calculated from the $x-y$ Fourier transform of the initial conditions in displacement $\tilde{u}_i^0(k_x,k_y,z)$. In the same way, weights $W_1(k_x,k_y)$ are calculated from the $x-y$ Fourier transform of the initial conditions in velocity $\tilde{v}_i^0(k_x,k_y,z)$. In (equation (B4)) we have considered that the eigenfunctions are orthogonal. The orthogonality is demonstrated in the in-plane case by *Favreau et al.* [1999], and this result can be extended to the 3-D study. Therefore we can use a technique of normalized projection of the initial conditions on the eigenfunctions and we find

$$W_0(k_x \cdot k_y) = \frac{1}{N(k_x,k_y)}\int_0^{+\infty}\sum_{i=x,y,z}\left((u_i^{k_x,k_y})^*(z)\tilde{u}_i^0(k_x,k_y,z)\right)dz, \quad (B5)$$

where

$$N(k_x,k_y) = 4\pi^2\int_0^{+\infty}\sum_{i=x,y,z}\left((u_i^{k_x,k_y})^*(z)u_i^{k_x,k_y}(z)\right)dz$$
$$= \frac{2\pi^2}{sp}\left(s^2k_x^2(4s(k_x^2+p^2) - 5p(s^2+k_x^2)) + p(s^6+k_x^6)\right)$$
$$+ \frac{2\pi^2}{sp}k_y^2\left(4s^3k_x^2 + p(k_y^2(s^2+k_x^2) + 2(k_x^4-s^4) - 4s^2k_x^2)\right). \quad (B6)$$

Appendix C: W_1 for a Narrow Gaussian Velocity Perturbation

[30] For a perturbation of the velocity field of half-width a defined by $v_x^0(x,y,z) = v_0e^{-(x^2+y^2+z^2)/a^2}$, we have

$W_1(k_x,k_y)$
$$= \frac{v_0 s\pi^{\frac{3}{2}}a^3 e^{-(k_x^2+k_y^2)a^2/4}(-2k_x^2 e^{-p^2a^2/4}\text{Erfc}(\frac{pa}{2}) + (s^2+k_x^2-k_y^2)e^{-s^2a^2/4}\text{Erfc}(\frac{sa}{2}))}{2N(k_x,k_y)}, \quad (C1)$$

where Erfc is the complementary error function.

Appendix D: Time of Initiation of the Infinite Fault

[31] For a narrow perturbation of characteristic half-width a we can estimate the time of initiation T_c to reach the critical slip $2L_c$ on the fault. For this purpose we write the simplified expression of $u_x^d(t,x,y,0)$ on the fault due to a perturbation of displacement $u_x^0(x,y,z)$ and velocity $v_x^0(x,y,z)$. We get

$$u_x^d(t,x,y,0) = \frac{1}{v_s^2}\int\int_{D_s}s\lambda^2 e^{i(k_xx+k_yy)}$$
$$\cdot \left(W_0(k_x,k_y)\cosh(\lambda t) + \frac{W_1(k_x,k_y)}{\lambda}\sinh(\lambda t)\right)dk_xdk_y. \quad (D1)$$

For a narrow perturbation, i.e., $a\alpha_c \ll 1$, we can take the following approximation for equation (B5):

$$W_0(k_x,k_y) \approx W_0(0,0)$$
$$= \frac{1}{2\pi\alpha_c^2}\int_0^{+\infty}\int_{-\infty}^{+\infty}\int_{-\infty}^{+\infty}u_x^0(x,y,z)e^{-\alpha_cz}dxdydz. \quad (D2)$$

The same approximation can be applied to $W_1(k_x, k_y)$ by taking $v_x^0(x,y,z)$ instead of $u_x^0(x,y,z)$ in equation (D2).
[32] If $\lambda(0,0)T_c \gg 1$, i.e., $T_c \gg 1/(\alpha_cv_s)$, we can use other approximations. The slip is driven by the most dominant eigenfunction, i.e., the one for which $k_x = k_y = 0$. The integrand is null on ∂D_s because the corresponding eigenfunctions are null. Therefore the integrand in equation (D1) is approximated linearly on each radius in the $x-y$ Fourier domain. Consequently, the integration over D_s in equation (D1) corresponds to the volume of a cone. Its base is D_s, and its height is the value of the integrand at $k_x = k_y = 0$. The surface of D_s is $\frac{\pi\alpha_c^2(\gamma+1)}{2\gamma^{3/2}}$. We also use $\cosh(a)\overset{a\to+\infty}{\longrightarrow}\sinh(a)\overset{a\to+\infty}{\longrightarrow}\frac{e^a}{2}$. By applying all of this to equation (D1), we obtain

$$u_x^d(T_c,0,0,0) = \frac{1}{v_s^2}\frac{1}{3}$$
$$\cdot \frac{\pi\alpha_c^2(\gamma+1)}{2\gamma^{3/2}}v_s^2\alpha_c^3\left(W_0(0,0) + \frac{W_1(0,0)}{v_s\alpha_c}\right)\frac{e^{v_s\alpha_cT_c}}{2}. \quad (D3)$$

By identifying $u_x^d(T_c, 0, 0, 0)$ with L_c, we have

$$T_c = \frac{1}{\alpha_cv_s}\ln\left(\frac{L_c}{\frac{\pi\alpha_c^5(\gamma+1)}{12\gamma^{3/2}}\left(W_0(0,0) + \frac{W_1(0,0)}{v_s\alpha_c}\right)}\right). \quad (D4)$$

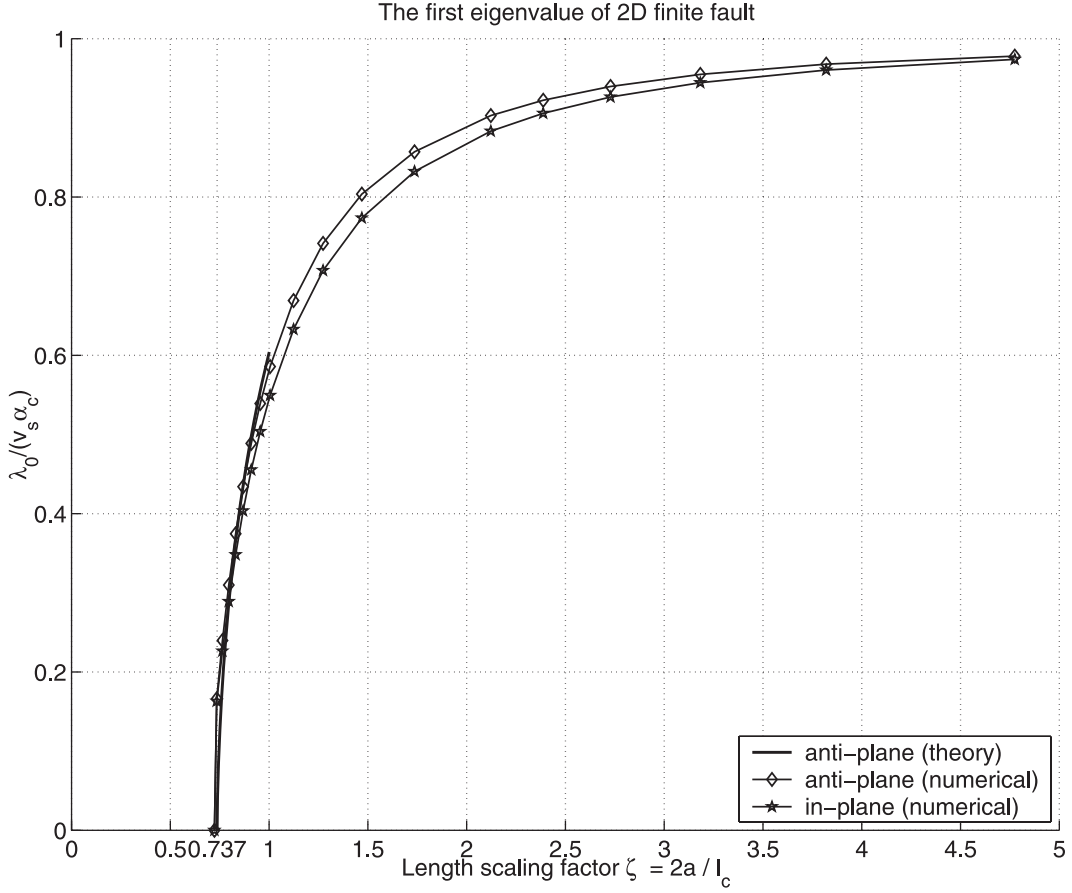**Figure E1.** The first eigenvalue for 2-D finite faults as a function of the length scaling factor ζ.

For a narrow Gaussian perturbation of the velocity field of half-width a defined by $v_x^0(x,y,z) = v_0 e^{-(x^2+y^2+z^2)/a^2}$, we have

$$W_1(0,0) = \frac{v_0 a^3}{4\pi^{\frac{1}{2}}\alpha_c^2} e^{-\alpha_c^2 a^2/4} \text{Erfc}\left(\frac{\alpha_c a}{2}\right), \qquad (D5)$$

and finally

$$T_c = \frac{1}{\alpha_c v_s}\left(\ln\left(\frac{48\gamma^{3/2}}{\pi^{1/2}(\gamma+1)\alpha_c^2 a^2}\frac{L_c v_s}{a v_0}\frac{1}{\text{Erfc}(\frac{\alpha_c a}{2})}\right) + \frac{\alpha_c^2 a^2}{4}\right). \quad (D6)$$

With $\rho = 3000\ \text{kgm}^{-3}$, $v_s = 3333\text{ms}^{-1}$, $\sigma_s - \sigma_d = 10\text{MPa}$, and $L_c = 0.18$ m one obtains $\alpha_c = 0.0017\text{m}^{-1}$. Moreover, with $\eta = v_p/v_s = \sqrt{3}$, i.e., $\gamma = 2(1-1/\eta^2) = 4/3$, $a = 200\text{m}$, and $v_0 = 0.0001\text{ms}^{-1}$, formula (Dg) gives $T_c = 2.81\text{s}$.

Appendix E: Link With the 2-D Results

[33]   In two dimensions (antiplane and in-plane) an elementary 2-D finite fault is a slip-weakening segment of length $2a$ limited by barriers of infinite strength (no slip in the barrier). This segment has a rate of weakening α_c. We have studied the influence of the finiteness numerically [*Ionescu and Campillo*, 1999] and theoretically [*Dascalu et al.*, 2000] for the antiplane finite fault. The spectral properties of the antiplane finite fault can be summarized

in two points. First, when the product $\beta = a\alpha_c$ of the fault half length a with the weakening parameter α_c is less than $\beta_0 = 1.15777\ldots$, then the eigenvalue analysis gives no real positive λ, and the fault is stable. Second, when this product is larger than β_0 (i.e., $\beta > \beta_0$), there exists a discrete collection of real positive eigenvalues $\lambda_n(\beta)_{,n \in N}$. The total number of positive eigenvalues grows with β. The first and largest one, $\lambda_0(\beta)$, gives the characteristic exponent of the slip growth (i.e., the slip grows like $e^{\lambda_0 t}$), and it makes it possible to give naturally an order of magnitude of the time of initiation. Indeed, the time of initiation is inversely proportional to λ_0. The calculation of $\lambda_0(\beta)$ as a function of β has been performed by *Dascalu et al.* [2000] near the stability, i.e., for real eigenvalue such that $1/|\lambda|$ is greater than the characteristic wave travel time a/v_s. This analysis has been compared with finite-difference computations. For large β the maximum eigenvalue tends theoretically to $v_s\alpha_c$, which corresponds to the maximum eigenvalue of the antiplane infinite fault [see *Campillo and Ionescu*, 1997]. In the in-plane geometry we found similar results, but we have no equivalent results like the one of *Dascalu et al.* [2000] in the antiplane case. The general spectral properties should be similar as in the antiplane problem. The limit of stability is given theoretically by $\beta > 2(1-1/\eta^2)\beta_0$. For large β the maximum eigenvalue tends theoretically to $v_s\alpha_c$, which corresponds to the maximum eigenvalue of the in-plane infinite fault [see *Favreau et al.*, 1999].

[34] To make a clear link between the present 3-D canonical fault study and the previous 2-D studies, let us define $\zeta = 2a/l_c$, where l_c is the length of the 2-D slipping patch ($l_c = \pi/\alpha_c$ in the antiplane case and $l_c = 2(1-1/\eta^2)\pi/\alpha_c$ in the in-plane case). With this definition we have the relations $\zeta = (2/\pi)\beta$ in antiplane and $\zeta = \frac{1}{\pi(1-1/\eta^2)}\beta$ in plane. In terms of parameter ζ the position of the critical point is independent of the value of the P wave velocity. Therefore antiplane and in-plane problems have the same critical point at $\zeta_0 = 0.7370\ldots$. In addition, since the maximal eigenvalue in all homogeneous infinite shear problem is $v_s\alpha_c$, we propose to represent systematically the dimensionless eigenvalue $\lambda_0(\zeta)/(v_s\alpha_c)$. In Figure E1, we plot the eigenvalue found by *Dascalu et al.* [2000] using this new notation for antiplane faults. We also plot our finite-difference numerical results for in-plane finite faults. Finally, in the 2-D and in the 3-D studies, parameter ζ takes the same sense; that is, it is the length scaling factor of the finite fault compared to the slipping patch of the infinite fault. The value of $\lambda_0(\zeta)/(v_s\alpha_c)$ is the ratio of the first eigenvalue of the finite fault to the largest one of the infinite fault.

References

Andrews, D. J., Rupture propagation with finite stress in anti-plane strain, *J. Geophys. Res*, 81, 3575–3582, 1976a.

Andrews, D. J., Rupture velocity of plain strain shear crack, *J. Geophys. Res*, 81, 5679–5687, 1976b.

Campillo, M., and I. R. Ionescu, Initiation of an antiplane shear instability under slip-dependent friction, *J. Geophys. Res.*, 102, 20,363–20,371, 1997.

Campillo, M., P. Favreau, I. R. Ionescu, and C. Voisin, On the effective friction law of an heterogeneous fault, *J. Geophys. Res*, 106, 16,307–16,322, 2001.

Dascalu, C., I. R. Ionescu, and M. Campillo, Fault finiteness and initiation of dynamic shear instability, *Earth Planet. Sci. Lett.*, 177, 163–176, 2000.

Dieterich, J. H., Earthquake nucleation on faults with rate-and-state dependent strength, *Tectonophysics*, 211, 115–134, 1992.

Ellsworth, W. L., and G. C. Beroza, Seismic evidence for an earthquake nucleation phase, *Science*, 268, 851–855, 1995.

Favreau, P., M. Campillo, and I. R. Ionecu, Initiation of in-plane shear instability under slip-dependent friction, *Bull. Seismol. Soc. Am.*, 89, 1281–1295, 1999.

Ida, Y., Cohesive force along the tip of a longitudinal shear crack and Griffith's specific surface energy, *J. Geophys. Res.*, 77, 3796–3805, 1972.

Iio, Y., Slow initial phase of the P-wave velocity pulse generated by micro-earthquakes, *Geophys. Res. Let.*, 19, 477–480, 1992.

Iio, Y., S. Ohmi, R. Ikeda, E. Yamamoto, H. Ito, H. Sato, Y. Kuwahara, T. Ohminato, B. Shibazaki, and M. Ando, Slow initial phase generated by microearthquakes occurring in the western Nagano prefecture, Japan—The source effect, *Geophys. Res. Lett.*, 26, 1972–1979, 1999.

Ionescu, I. R., and M. Campillo, Influence of the shape of the friction law and fault finiteness on the duration of initiation, *J. Geophys. Res.*, 104, 3013–3024, 1999.

Knopoff, L., J. Landoni, and M. Abinante, The causality constraint for fractures with linear slip weakening, *J. Geophys. Res.*, 105, 28,035–28,043, 2000.

Madariaga, R., K. Olsen, and R. Archuleta, Modeling dynamic rupture in 3-D earthquake fault model, *Bull. Seismol. Soc. Am.*, 88, 1182–1197, 1998.

Matsu'ura, M., H. Kataoka, and B. Shibazaki, Slip-dependent friction law and nucleation processes in earthquake rupture, *Tectonophysics*, 211, 135–148, 1992.

Ohnaka, M., Non-uniformity of the constitutive law parameters for shear rupture and quasistatic nucleation to dynamic rupture: A physical model of earthquake generation model, *Proc. Natl. Acad. Sci. U.S.A.*, 93, 3795–3802, 1996.

Ohnaka, M., and L. Shen, Scaling of the shear rupture process from nucleation to dynamic propagation: Implication of geometry irregularity of the rupturing surfaces, *J. Geophys. Res.*, 104, 817–844, 1999.

Ohnaka, M., Y. Kuwahara, and K. Yamamoto, Constitutive relations between dynamic physical parameters near a tip of the propagation slip during stick-slip shear failure, *Tectonophysics*, 144, 109–125, 1987.

Olsen, K., R. Madariaga, and R. Archuleta, Three dimensional dynamic simulation of the 1992 Landers earthquake, *Science*, 278, 834–838, 1997.

Peyrat, S., K. Olsen, and R. Madariaga, Dynamic modeling of the 1992 Landers earthquake, *J. Geophys. Res.*, 106, 26,467–26,482, 2001.

Rice, J. R., and A. L. Ruina, Stability of steady frictional slipping, *J. Appl. Mech.*, 50, 343–349, 1983.

Rice, J. R., Spatio-temporal complexity of slip on a fault, *J. Geophys. Res.*, 98, 9885–9907, 1993.

Shibazaki, B., and M. Matsu'ura, Transition process from nucleation to high-speed rupture propagation: Scaling from stick-slip experiments to natural earthquakes, *Geophys. J. Int.*, 132, 14–30, 1998.

Voisin, C., M. Campillo, I. R. Ionescu, F. Cotton, and O. Scotti, Dynamic versus static stress triggering and friction parameters: Inference from the November 23, 1980, Irpinia earthquake, *J. Geophys. Res.*, 105, 22,647–22,659, 2000.

————————

P. Favreau and M. Campillo, Laboratoire de Géophysique Interne, Observatoire de Grenoble, Université Joseph Fourier, Cedex, France.

I. R. Ionescu, Laboratoire de Mathématiques Appliquées, Université de Savoie, Campus Scientifique, Cedex, France.